Plant Stress 22 (2026) 101464

Contents lists available at ScienceDirect

Plant Stress

journal homepage: www.sciencedirect.com/journal/plant-stress

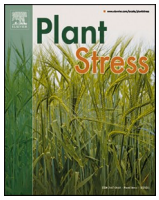

Unravelling the protective role of silicon in *Cannabis sativa* hypocotyls under cadmium and zinc stress with imaging and *-omics*

Roberto Berni [a], Céline C. Leclercq [a], Sébastien Planchon [a], Václav Motyka [b], Petre I. Dobrev [b], Sergio Sorbo [c], Adriana Basile [d], Jenny Renaut [a], Stanley Lutts [e], Gea Guerriero [a,*]

[a] *Luxembourg Institute of Science and Technology, 5, rue Bommel, 4940, Hautcharage, Luxembourg*
[b] *Institute of Experimental Botany, The Czech Academy of Sciences, Rozvojová 263, 16502, Prague 6, Czech Republic*
[c] *University Federico II, CeSMA, Microscopy section, via Cinthia, 80126, Naples, Italy*
[d] *University Federico II, Biology Department, via Cinthia, 80126, Naples, Italy*
[e] *Groupe de Recherche en Physiologie Végétale (GRPV), Earth and Life Institute–Agronomy (ELI-A), Université Catholique de Louvain, Croix du Sud 45, boîte L7.07.13, 1348, Louvain-la-Neuve, Belgium*

A R T I C L E I N F O

Keywords:
Cannabis sativa
Potentially toxic elements
Silicon
Imaging
-Omics

A B S T R A C T

Potentially toxic elements (PTEs) such as cadmium (Cd) and zinc (Zn) are environmental pollutants affecting soil quality and plant growth. Cd is a highly toxic element primarily introduced into the environment through anthropogenic activities. The impact of Cd on plants is particularly severe, as it disrupts cellular metabolism. Zn, conversely, is an essential micronutrient required for several enzymatic functions, including those involved in DNA synthesis, protein production, and oxidative stress regulation. However, excessive Zn levels in soils can lead to toxic effects on plants. The multi-purpose crop hemp (*Cannabis sativa* L.) has gained attention for its ability to tolerate and accumulate PTEs, including Cd and Zn. In this study, the impact of Cd and Zn with and without the beneficial metalloid silicon (Si) was evaluated on 20-day-old hemp plantlets, focusing on the hypocotyl as a model for bast fibre formation. An integrative approach combining microscopy and multi-*omics* was applied. The results showed that Cd and Zn impaired bast fibre organisation and disrupted cell wall ultrastructure, causing an altered tissue architecture. Si mitigated these effects by preserving cell wall structure and stabilising secondary wall components. At the molecular level, Si enhanced apoplastic reinforcement through the activation of hemicellulose biosynthesis and cell wall-associated proteins. In addition, Si improved redox homeostasis by stimulating glutathione-dependent detoxification under Cd stress and supported energy metabolism under Zn exposure. Hormonal profiling indicated that Si modulated stress responses by maintaining cytokinin signalling while attenuating ABA- and JA-mediated pathways. The data obtained revealed specific responses at the tissular, ultrastructural and molecular levels, highlighting the beneficial role of Si in mitigating the effects of Cd and Zn.

1. Introduction

The contamination of soils by potentially toxic elements (PTEs, i.e., naturally occurring or anthropogenic elements that persist in the environment and may exert toxic effects depending on their concentration and bioavailability) is an issue of increasing environmental concern that is largely driven by industrial activities, mining operations, waste disposal and agricultural practices (Ondrasek et al., 2025). Among the various PTEs, cadmium (Cd) and zinc (Zn) are of particular concern due to their persistence, mobility, and capacity to adversely affect ecological systems and human health (Rasin et al., 2025; Meng et al., 2023).

While Zn is an essential micronutrient required for plant and animal metabolism, excessive concentrations can impair biological processes, nutrient cycling and soil microbial communities (Van et al., 2024). Cd toxicity results in stunted growth, chlorosis, reduced biomass and significant damage to cellular organelles, especially chloroplasts, which impairs photosynthetic efficiency (Soni et al., 2024).

Both PTEs, when present in excessive concentrations, share common mechanisms of toxicity, including the disruption of nutrient homeostasis, interference with photosynthesis and metabolic pathways, and oxidative damage caused by the overproduction of reactive oxygen species (ROS) (Lin and Aarts, 2012). Plants mitigate this stress through

* Corresponding author.
E-mail address: gea.guerriero@list.lu (G. Guerriero).

https://doi.org/10.1016/j.stress.2026.101464
Received 5 February 2026; Received in revised form 9 June 2026; Accepted 30 June 2026
Available online 30 June 2026

the activation of antioxidant defence systems, including enzymes, such as superoxide dismutase, catalase and peroxidases, as well as non-enzymatic antioxidants, such as glutathione and ascorbate (Berni et al., 2018).

Textile hemp (*Cannabis sativa* L.), a versatile and economically relevant crop grown for its cellulosic bast fibres, nutrient-rich seeds and medicinal compounds (Andre et al., 2016), has gained attention for its ability to tolerate and accumulate PTEs, among which Cd and Zn (Nash et al., 2024; Luyckx et al., 2021; Luyckx et al., 2021; Luyckx et al., 2023; Berni et al., 2024). These characteristics position hemp as a promising candidate for phytoremediation (Lavanya et al., 2024).

Both Cd and Zn were shown to inhibit *C. sativa* plants' growth and modify the proteome, through Cd-induced stress responses, such as the activation of phytochelatin synthesis and oxidative stress-related pathways (Luyckx et al., 2021). At the bast fibre level, both PTEs reduced the diameter of primary fibres, altered crystalline cellulose distribution, as well as the expression of cell wall-related genes (Berni et al., 2024). Cd preferentially accumulated in roots (Berni et al., 2024; Androudi et al., 2024), consistent with the upregulation of genes involved in root sequestration and xylem transport (Marabesi et al., 2023).

The metalloid silicon (Si) has been defined as quasi-essential for plant growth and development (Manivannan et al., 2023) in the light of its positive effects on different species exposed to a wide range of (a) biotic stressors (Berni et al., 2021, Huang et al., 2024; Shen et al., 2022; Celayir et al., 2023; Yang et al., 2022; Song et al., 2024). When applied to hemp exposed to Cd, Si reduced accumulation in plant tissues, improved water-use efficiency and enhanced thiol-based detoxification through glutathione and phytochelatin synthesis (Luyckx et al., 2021); Si also restored bast fibres' diameter (Luyckx et al., 2021).

Despite extensive research (Luyckx et al., 2021; Luyckx et al., 2021; Luyckx et al., 2023; Berni et al., 2024; Luyckx et al., 2021; Marabesi et al., 2023), several aspects of the hemp response to Cd and Zn stress in the presence of Si remain poorly understood, particularly regarding the integration of molecular, structural, and physiological changes, largely due to the limited availability of integrated, multi-level datasets. Comprehensive datasets combining transcriptomics, proteomics and imaging are still limited, hindering the ability to establish direct links between these biological levels and making it difficult to fully elucidate the mechanisms underlying bast fibre development, stress tolerance and cell wall remodelling in PTEs- and Si-treated hemp. To address these gaps, the present study focussed on *C. sativa* hypocotyl, a well-established model system for investigating bast fibre cell wall biogenesis due to its clear temporal separation between elongation and secondary thickening phases (Berni et al., 2024; Behr et al., 2016). It is hypothesised that Si mitigates Cd and Zn toxicity by coordinating molecular, structural and physiological responses that ultimately preserve cell wall integrity and function in bast fibres. Accordingly, the objectives of this study were to: (1) characterise the structural and ultrastructural modifications of hypocotyl tissues under Cd and Zn stress, in the presence or absence of Si, using immunohistochemistry and transmission electron microscopy (TEM); (2) investigate the underlying molecular responses through transcriptomic (RNA-Seq) and cell wall proteomic analyses; and (3) assess associated physiological and metabolic adjustments, including hormonal profiling, to elucidate how these changes contribute to Si-mediated protection.

By combining these complementary approaches, this study aims to establish a mechanistic link between PTE-induced molecular alterations and their structural and functional consequences in bast fibres, thereby providing a more comprehensive understanding of the adaptive responses of textile hemp to Cd and Zn stress.

2. Materials and methods

2.1. Cultivation of textile hemp, biomass quantification and elemental analysis

Seeds of *C. sativa* (monoecious var. Santhica 27 purchased from the French cooperative Hemp-it) were grown in potting soil with vermiculite (to improve water retention; 1 kg mixed with 7 kg of soil) containing $CdCl_2$ (28.5 mg/kg) and $ZnCl_2$ (46 mg/kg) in the presence and absence of $Na_2SiO_3{\cdot}5H_2O$ (0.36 g/kg). The concentrations of PTEs were selected based on an earlier study (Berni et al., 2024). The concentration of Na_2SiO_3 corresponded to 1.7 mM and was selected to ensure physiologically relevant Si availability without exceeding the solubility limit of Si.

The potting soil consisted of a mixture of 1/3 sand and 2/3 peat moss (Compo, Deinze, Belgium), supplied as a commercial substrate containing perlite and a basal fertiliser.

Four experimental treatments were established: (1) control (no PTEs, no Si), (2) no PTE with Si supplementation, (3) PTEs (Cd or Zn) without Si, and (4) PTEs (Cd or Zn) with Si supplementation. $CdCl_2$, $ZnCl_2$ and $Na_2SiO_3{\cdot}5H_2O$ were obtained from Sigma-Aldrich (Germany). $CdCl_2$ and $ZnCl_2$ were dissolved in water and thoroughly homogenised into the soil substrate to ensure uniform distribution of the contaminants. The soil was then spread and air-dried overnight to stabilise PTE incorporation. To prevent direct exposure of germinating seeds to high metal concentrations, seeds were sown in a 1.5-cm top layer of uncontaminated potting soil placed above the contaminated substrate. Plants were then transferred to controlled growth chambers set at 60% relative humidity with a photoperiod of 16 h light (7000 lux) at 25°C, 60% relative humidity and 8 h dark at 20°C. The positions of the plants were randomised on a weekly basis to prevent bias arising from fixed locations within the growth chamber. Plants were watered twice a week by adding 100 ml tap water to each pot, following the protocol described in Berni et al. (2024) and ensuring consistent soil moisture across all treatments, sufficient to sustain plant growth while avoiding waterlogging, as indicated by the absence of standing water or drainage from the pots and the maintenance of a well-aerated, non-compacted substrate. No additional fertiliser was applied during the experiment to avoid potential interactions between nutrient availability and PTE uptake. For the molecular analyses, 2 cultivation batches were prepared under identical conditions: the first dedicated to transcriptomics, in which 3 biological replicates were used, and the second for gel-free proteomics, elemental analysis and hormonomics, in which 4 biological replicates were prepared. Each biological replicate was composed of 3 plants and harvested 20 days (d) after sowing. A third cultivation batch with 3 biological replicates was dedicated to microscopy and biomass yield quantification. The number of biological replicates was selected to ensure adequate representation of biological variability within each dataset, while accounting for the distinct technical variability and resource constraints associated with the different analytical platforms. The fresh weight (FW) was recorded immediately after harvest, while the dry weight (DW) was determined following 72 h of lyophilisation.

2.2. Elemental analysis

Lyophilised and ground leaves, roots, epicotyls, as well as soil samples were digested by microwave-assisted mineralisation (Multiwave Pro, Anton Paar, Graz, Austria), according to the procedure previously reported (Berni et al., 2024). Digests were brought to 25 ml with ultrapure water, centrifuged (4700 rpm, 10 min), filtered (0.2 µm PTFE; Merck Millipore, Darmstadt, Germany), and stored at 4°C prior to analysis. Si, Cd and Zn concentrations were determined by ICP-MS (Agilent 7900; Agilent Technologies, Santa Clara, CA, USA) after appropriate dilution, using a calibration range of 100-2500 $\mu g{\cdot}l^{-1}$ for ^{28}Si, 0.25-2500 $\mu g{\cdot}l^{-1}$ for ^{66}Zn, and 0.025-250 $\mu g{\cdot}l^{-1}$ for ^{111}Cd. Blanks and quality controls were included every 10 samples, with ^{103}Rh and

^{185}Re as internal standards. Results were corrected for dilution and certified reference material recovery (*Citrus* leaves, NCS ZC 73018; China National Analysis Center for Iron and Steel, Beijing, China) and expressed as $\mu g \cdot g^{-1}$ DW. Bioconcentration factors (BCF) were calculated as the ratio of PTE concentration in roots to that in the corresponding soil. Translocation factors (TF) were calculated as the ratio of PTE concentration in leaves to that in roots (Luyckx et al., 2021; Akkaya et al., 2025).

2.3. Optical and transmission electron microscopy

Plantlets aged 20 d were carefully removed from the soil, then hypocotyls were sampled with a sterile blade and quickly processed for microscopy (Olympus BX51, Tokyo, Japan, equipped with a Toupview camera and software, ToupTek Photonics, Zhejiang, China). Sample preparation for optical microscopy with subsequent staining and immunodetection followed the procedure detailed previously (Berni et al., 2024; Behr et al., 2016). The procedures to prepare the samples for Transmission Electron Microscopy and visualise them at the TEM microscope followed the method described earlier (Behr et al., 2019; Maresca et al., 2023). Small pieces of freshly excised tissue (ca. 2 mm) were immediately immersed in a buffered fixative containing glutaraldehyde 2% v/v and paraformaldehyde 1.6% v/v in phosphate buffer, pH 7.2 to preserve cellular architecture, followed by post-fixation in osmium tetroxide 1% w/v to improve membrane contrast. After rinsing in buffer, samples were dehydrated through a graded ethanol series consisting of 10%, 30%, 50%, 70% and 100% ethanol (v/v), with each step carried out sequentially to ensure gradual water removal and minimise structural damage. Dehydrated tissues were then infiltrated and embedded in Spurr's epoxy medium (Agar Scientific Ltd, Stansted, Essex, UK) and polymerised under controlled T conditions (70°C). Ultrathin sections (60 nm) were obtained using a Supernova ultramicrotome (Reichert-Jung, Wien, Austria), mounted onto copper grids and stained with uranyl acetate followed by lead citrate to enhance contrast. Sections were examined using an EM208S TEM (Philips, Eindhoven, The Netherlands) operated at 80 kV as an accelerating voltage, allowing detailed observation of subcellular features within the stem tissues.

2.4. Quantification of plant hormones

The epicotyls were quickly excised, plunged in liquid nitrogen and reduced to a fine powder with a mortar and pestle. Subsequently, the samples were transferred to pre-frozen tubes (Eppendorf, Hamburg, Germany) and stored at -80°C until the analyses. Phytohormone analysis was performed as described in Schmidt et al. (2024). Approximately 20 mg of fresh plant material was homogenised with 1.5-mm zirconium beads, 100 µl of 1 M HCOOH in water, and a mixture of internal standards using a FastPrep-24 instrument (MP Biomedicals, CA, USA). After centrifugation at 17,500 rpm for 20 minutes and re-extraction, the combined supernatant was applied to an Oasis HLB 10 mg, 96-well solid-phase extraction (SPE) plate (Waters Corporation, Milford, MA, USA). The supernatant was pressed through the SPE plate using a Pressure+96 manifold (Biotage, Uppsala, Sweden). The SPE plate was then washed three times with 100 µl of water. Samples were eluted with 100 µl of a 1:1 acetonitrile/water solution (v/v). An aliquot of the eluate was injected into an LC-MS system consisting of a UHPLC 1290 Infinity II (Agilent Technologies, Santa Clara, CA, USA) coupled with a 6495 triple quadrupole mass spectrometer (Agilent Technologies). MS analysis was performed in MRM mode with two transitions per compound using an isotope dilution method. Data acquisition and processing were performed using Mass Hunter Software B.08 (Agilent Technologies).

2.5. RNA-Seq and qPCR analysis

RNA was extracted from the hypocotyls as previously reported (Berni et al., 2024). Libraries were prepared with the KAPA HyperPrep Kit (Roche, Basel, Switzerland) following the manufacturer's instructions (Xu et al., 2023) and sequenced on an Illumina NextSeq2000 (Illumina Inc., San Diego, CA, USA) with a P2 XLEAP-SBS flow cell (100 cycles). Processing of the reads imported in pairs was carried out as previously reported (Xu et al., 2023). Briefly, reads were quality-filtered (length >35 bp, default quality score of 0.05), trimmed to remove adapters and low-quality ends and mapped to the Santhica 27 transcriptome (Behr et al., 2019) using mismatch cost=2, insertion and deletion cost=3 and length and similarity fraction=0.8. Raw sequences were deposited at the Sequence Read Archive (SRA) with the accession number PRJNA1358720. Hierarchical clustering of the expression values (presented as heatmaps) was obtained with Cluster 3.0 (Eisen et al., 1998) and visualised with Java Treeview (Saldanha, 2004). To validate the RNA-Seq data, a set of 8 genes was selected. The qPCR was performed as previously reported (Berni et al., 2024) using a ViiA 7 Real-Time PCR System (Thermo Fisher, Waltham, MA, USA). Primers were designed using Primer3Plus and checked with the OligoAnalyzer tool. Primers are reported in Supplementary File 1.

2.6. Gel-free proteomics

The cell wall protein extraction was performed by combining previously described protocols. Briefly, samples were first subjected to lysis and homogenisation following the procedure described in Berni et al. (2023), including incubation in lysis buffer and mechanical disruption. Then, cell wall protein fractionation was performed according to Printz et al. (2015), starting from 50 mg of hypocotyl tissue per condition. Protein digestion (50 µg of total protein per sample) was then carried out using the PreOmics iST protocol (PreOmics GmbH, Martinsried, Germany). Protein quantification was performed via the Bradford method (Bradford, 1976).

LC-MS analysis was performed using a NanoLC-425 Eksigent system coupled to a TripleTOF® 6600+ mass spectrometer (SCIEX, Framingham, MA, USA), following the previously reported method (Guerriero et al., 2021). MS/MS data were processed with Progenesis QI for Proteomics (v4.2, Waters, Milford, MA, USA) and protein identification was conducted via Mascot Daemon (v2.6.0, Matrix Science, London, UK) against UniProt_*Cannabis_sativa* (downloaded on 9th august 2023; 76, 798 sequences). The Mascot parameters were as follows: peptide tolerance of 20 ppm, fragment mass tolerance of 0.3 Da, max two missed cleavages, carbamido-methylation of cysteine as fixed modification and oxidation of methionine, N-terminal protein acetylation and tryptophan to kynurenine as variable modifications. Only the proteins identified with a significance Mascot-calculated confidence of 95%, two peptides, at least one unique per proteins and a p-value<0.05 were retained. The mass spectrometry proteomics data were deposited in the ProteomeXchange Consortium via the PRIDE (Vizcaíno et al., 2016) partner repository with the dataset identifier PXD060911. The identified accession numbers were submitted to UniProt's ID mapping tool using default settings. The corresponding protein sequences were downloaded in FASTA format and these sequences were subsequently analysed using DeepLoc 2.0 (High-throughput/Short output mode) to identify the predicted subcellular localisation (Thumuluri et al., 2022).

The protein abundances were visualised as hierarchical clustering of the heatmaps, as previously described for transcriptomics.

2.7. Statistics

Data were log10-transformed before analysis in SPSS v19 (IBM Corp., Armonk, NY, USA). Normality was tested with Shapiro-Wilk and homogeneity with Levene's test. Normally distributed, homogeneous data were analysed using one-way ANOVA with Tukey's post hoc test; non-normal and/or non-homogeneous data were evaluated with the Kruskal-Wallis test followed by Dunn's post hoc test.

3. Results and discussion

3.1. Biomass yield of hemp tissues

Leaves of plants exposed to CdSi and ZnSi showed a significantly higher FW compared to those treated with Cd and Zn alone (Fig. 1a). No significant differences were observed in epicotyls and roots across treatments. A similar trend was observed for the leaf DW of CdSi-treated plants which showed higher values than Cd-exposed ones (Fig. 1b), suggesting that Si supplementation mitigated the growth inhibition caused by Cd in the aerial tissues. No significant differences were observed across treatments in the epicotyls.

In the roots, Si supplementation led to a significant decrease in DW under all conditions compared to C, Cd and Zn alone. It was reported that plants exposed to PTEs and treated with Si increased the root biomass (An et al., 2022; Mišúthová et al., 2021). The reduction in root DW observed under Si supplementation in hemp, even in the absence of PTEs, may be explained by a functional substitution of organic cell wall polymers with silica (SiO_2) deposits. Si is accumulated as amorphous SiO_2 within the apoplast (Guerriero et al., 2016): this mineral deposition can provide mechanical support and lead to a lower organic matter content per unit of tissue. However, without data on the cell wall composition of the hemp roots, such an explanation remains hypothetical.

It should also be noted that under CdSi and ZnSi a significant increased root biomass was observed compared to Si alone. The same applies under Cd treatment compared to C. This finding is in agreement with the previously reported increase in root biomass under Cd exposure in soil-grown hemp plantlets (Berni et al., 2024).

3.2. Elemental analysis in hemp tissues

In the absence of PTEs, Si accumulated at higher levels in leaves (with values between 7243-7468 $\mu g \cdot g^{-1}$ in the C and CSi conditions, respectively) in agreement with previous results (Guerriero et al., 2019) and roots (between 11787-15164 $\mu g \cdot g^{-1}$) compared to the epicotyls (between 3740-3788 $\mu g \cdot g^{-1}$) (Fig. 2a), indicating that Si uptake and deposition were more active in these tissues. The Si detected in all treatments most likely originated from the growth substrate, which consisted of a sand/peat mixture supplemented with vermiculite. Both sand and vermiculite contain silicate minerals; however, their contribution to plant-available Si is minimal due to their low solubility. In this respect it should be noted that bulk Si concentration, as determined by ICP-MS, does not capture the physiologically active fraction of Si nor its cellular localisation. Moreover, hemp is not a Si hyperaccumulator, in contrast to grasses such as rice. Under these soil-based conditions, Si can exert localised effects at the root surface and/or within the apoplast, without significantly altering total tissue Si content.

Under Zn exposure, root Si concentration decreased significantly with respect to to C and CSi, suggesting that Zn may impact Si uptake or transport, possibly through competitive interactions at the root membrane. High Zn supply was shown to reduce expression of the aquaporin

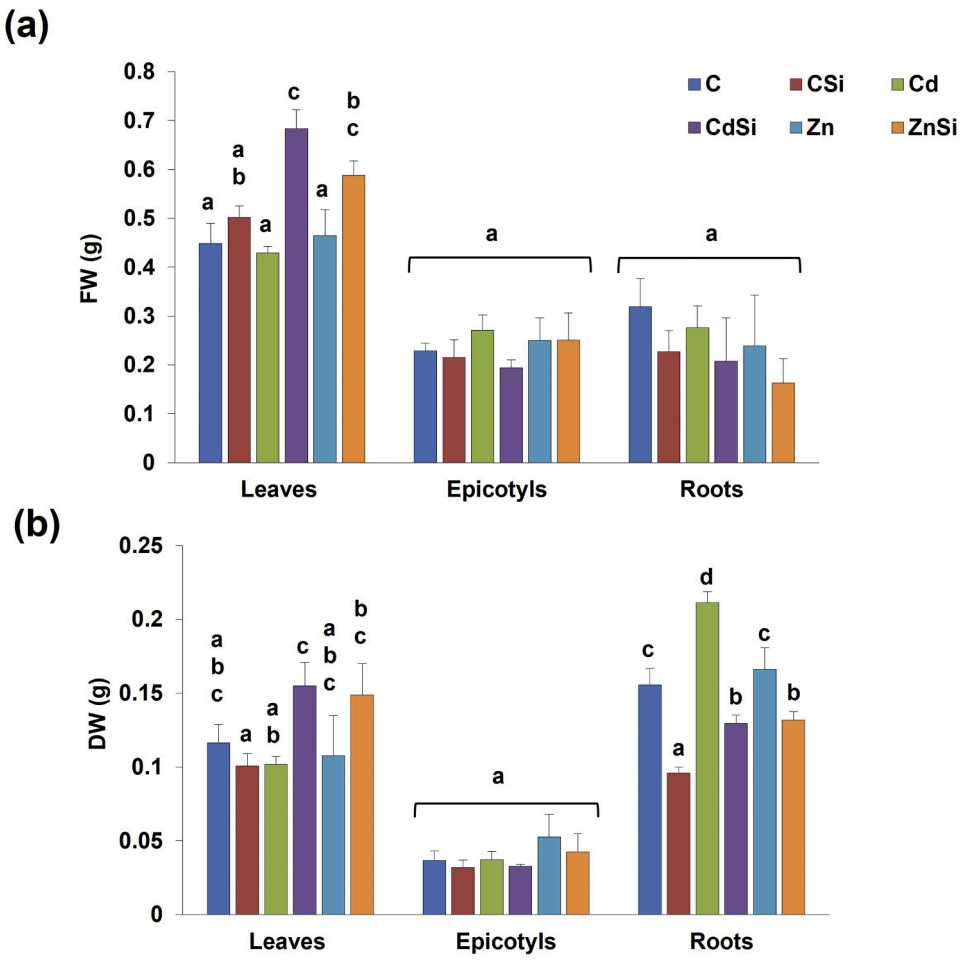

Fig. 1. Biomass accumulation reported as fresh-FW (a) and dry weight-DW (b) in *C. sativa* leaves, epicotyls, and roots in the absence and presence of Cd, Zn and Si. Data are the means of 3 biological replicates ±SD. Different letters indicate statistically significant differences among treatments within each tissue ($p<0.05$). C: samples under control conditions, CSi: samples exposed to Si, Cd: samples exposed to Cd, CdSi: samples exposed to Cd and Si, Zn: samples exposed to Zn, ZnSi: samples exposed to Zn and Si.

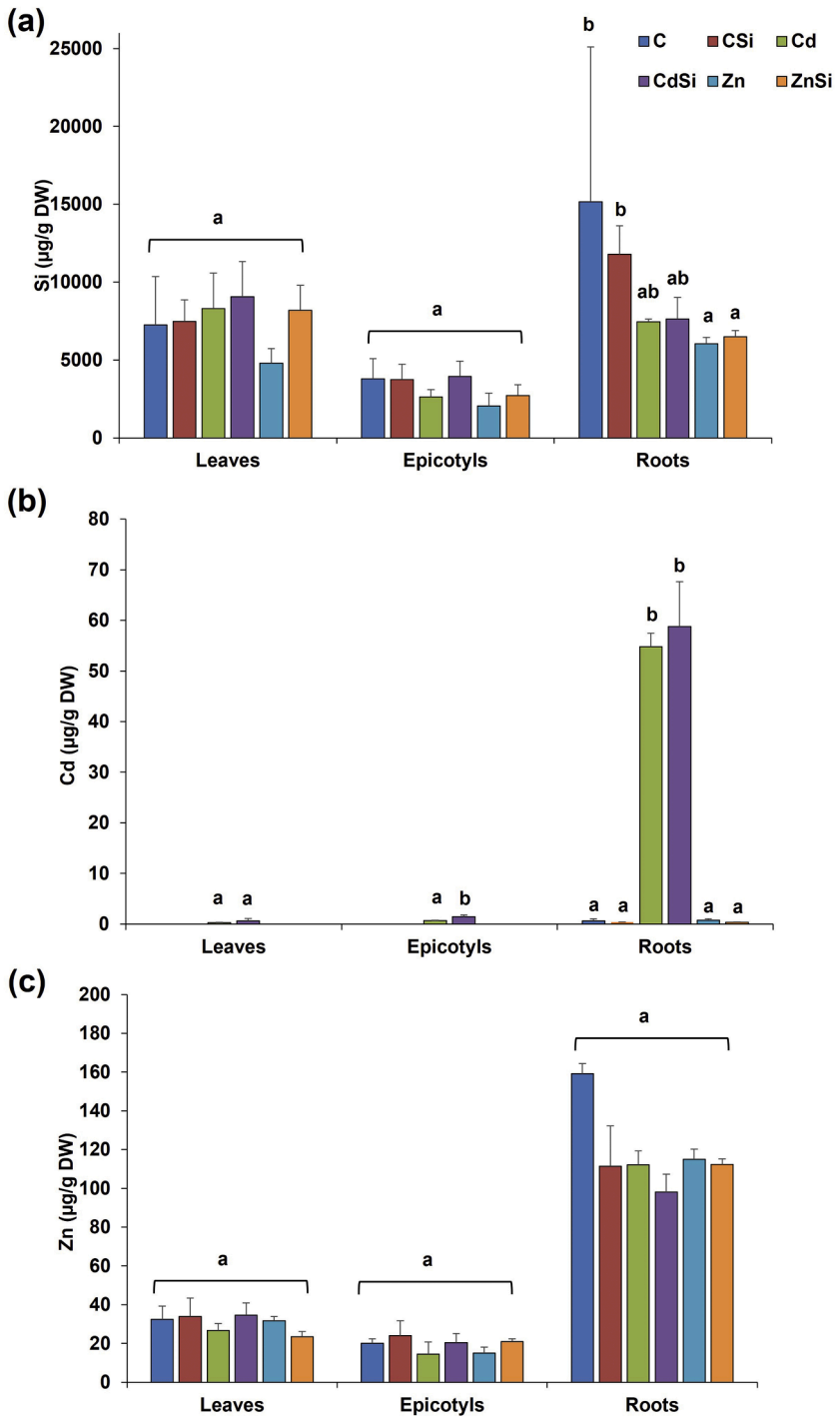

Fig. 2. Elemental analysis of Si (a), Cd (b) and Zn (c) in *C. sativa* leaves, epicotyls, roots in the absence and presence of Cd, Zn and Si. Data are the means of 3 biological replicates ±SD. Different letters indicate statistically significant differences among treatments within each tissue ($p<0.05$). C: samples under control conditions, CSi: samples exposed to Si, Cd: samples exposed to Cd, CdSi: samples exposed to Cd and Si, Zn: samples exposed to Zn, ZnSi: samples exposed to Zn and Si.

mediating Si uptake (*Lsi1*) in maize and to alter the root ionome, in agreement with competitive or regulatory interactions at the root membrane (Bokor et al., 2015).

Cd was predominantly accumulated in the roots (Fig. 2b), in agreement with previous findings (Luyckx et al., 2021; Berni et al., 2024), where its concentration was the highest among all tissues (between 54.8-58.8 $\mu g \cdot g^{-1}$ in the Cd and CdSi conditions, respectively), reflecting the limited translocation to aerial parts. The CdSi treatment was not significantly different from Cd alone in terms of content, suggesting that Si supplementation did not restrict Cd uptake or its movement within the plant under the tested conditions. In the epicotyls, Cd content was between 0.65-1.45 $\mu g \cdot g^{-1}$ in the Cd and CdSi conditions, respectively, while in the leaves it was between 0.25-0.60 $\mu g \cdot g^{-1}$. This is consistent with previous findings identifying the epicotyls as the secondary accumulation site for Cd in hemp after roots (Berni et al., 2024).

Zn accumulated at the highest level in the roots (between 112.2-115 $\mu g \cdot g^{-1}$ in the Zn and ZnSi conditions, respectively, without significant differences across treatments (Fig. 2c).

In parallel, the calculation of BCF and TF provided further insight into PTE partitioning. Under Cd exposure (soil Cd=17.72±1.99 $\mu g \cdot g^{-1}$),

a high root BCF (equivalent to 3.1±0.53) and extremely low TF (0.004 ±0.001) were observed, indicating strong Cd retention in roots. In the presence of CdSi (soil Cd=13.03±0.93 μg·g^{-1}), root BCF further increased (to 4.5±0.50), while TF remained low (0.005±0.001), supporting enhanced immobilisation of Cd in belowground tissues. A BCF greater than 1 indicates that the plant concentrates the PTE relative to the surrounding soil, whereas the very low TF demonstrates that only a negligible fraction of the accumulated PTE was translocated to the aerial tissues (Motrescu and Luchian, 2026; Huang et al., 2025). Therefore, hemp displayed a phytostabilisation rather than a phytoextraction strategy for Cd, with Si further reinforcing root sequestration.

In contrast, Zn exposure (soil Zn=126.68±7.8 μg·g^{-1}) and ZnSi treatment (soil Zn=120.85±4.9 μg·g^{-1}) showed BCF values close to unity (0.91±0.03 μg·g^{-1} for the condition with Zn and 0.93±0.05 μg·g^{-1} for the condition with ZnSi) and moderate TF values (0.20±0.02 μg·g^{-1} for the condition with Zn and 0.20±0.01 μg·g^{-1} for the condition with ZnSi). These values indicate that Zn uptake closely reflected its availability in the soil and that a proportion of the absorbed Zn was translocated to the aerial organs, in agreement with its role as an essential micronutrient. Unlike Cd, Si had only a limited effect on Zn partitioning, suggesting that its protective action primarily involved restricting the mobility of the toxic, non-essential element while preserving the physiological distribution of Zn.

3.3. *Immunohistological and ultrastructural changes in hemp hypocotyls*

The immunohistological analysis of hemp hypocotyls revealed structural and compositional changes influenced by the presence of Si, Cd, Zn alone and combined (Fig. 3).

Under Si supplementation and in the presence of Cd and Zn, the lumen of both primary and secondary bast fibres was wider. This morphological alteration, highlighted through optical and fluorescence microscopy with FASGA staining and the use of the crystalline cellulose epitope CBM3a (Fig. 3, top 3 rows), suggests that the supplementation of Si counteracted the typical swelling of the cell wall caused by PTEs such as Cd, previously reported in flax and hemp hypocotyls (Berni et al.,

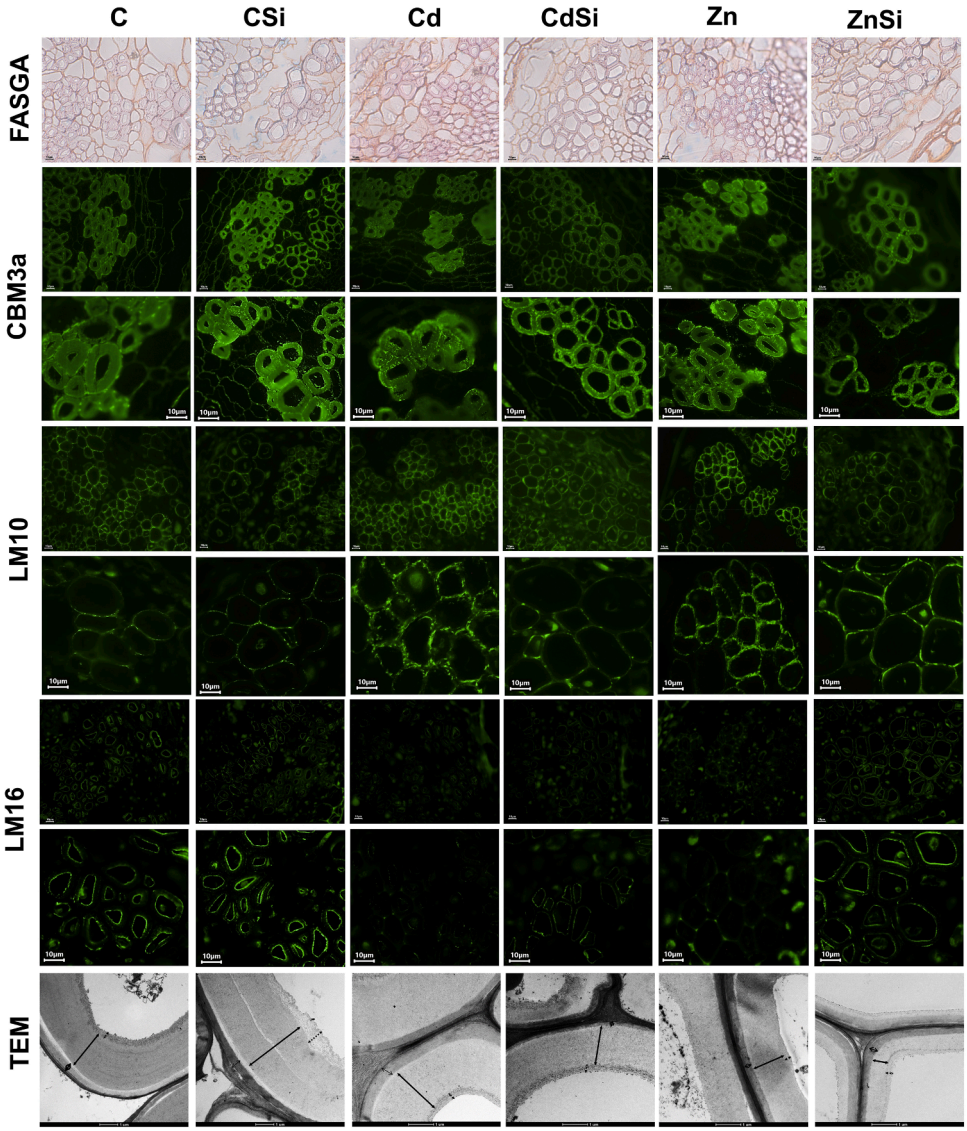

Fig. 3. Panel showing the hypocotyl sections under the different treatments at the optical, fluorescence and transmission electron microscope (TEM). The top row shows FASGA coloration; the 2nd and 3rd row display the distribution of crystalline cellulose detected with the CBM3a probe; the 4th and 5th row show the distribution of unsubstituted/low substituted xylan with the LM10 antibody; the 6th and 7th row indicate the distribution of arabinans detected with the LM16 antibody; in the last row, the bast fibres' ultrastructure is displayed, Scale bars indicate 10 μm in the images at the optical and fluorescence microscope and 1 μm in the TEM pictures. The thin double arrows indicate the S1-layer, the double arrows with filled tips the G-layer and the dotted double arrows the Gn-layer. C: samples under control conditions, CSi: samples exposed to Si, Cd: samples exposed to Cd, CdSi: samples exposed to Cd and Si, Zn: samples exposed to Zn, ZnSi: samples exposed to Zn and Si.

2024; Douchiche et al., 2011). A wider lumen reflects a reduction in aberrant cell wall swelling, indicating that Si helped maintain the mechanical integrity and organisation of bast fibres under PTE stress. This preservation of lumen space suggests that structural deformation was limited, thereby supporting the functional integrity of the fibres.

Xylan, detected using the LM10 antibody in the region corresponding to the S1-layer (Behr et al., 2019), showed a stronger signal under Cd and Zn exposure (Fig. 3, 4th and 5th rows). However, under Si supplementation, the increased LM10 signal was mitigated in intensity. The stronger xylan signal detected under Cd and Zn exposure suggests an increase in unsubstituted or low substituted xylan, as previously discussed by Luyckx and co-authors (Luyckx et al., 2021). Si mitigated this effect, as evidenced by the reduced xylan signal in the combined treatments. Si was shown to occur in hemp bast fibre cell walls (Guerriero et al., 2019), and its presence as SiO_2 may provide increased stiffness, in a manner analogous to unsubstituted/low substituted xylan.

The LM16 antibody targeting arabinan revealed uniform labelling in the inner region of the bast fibres under C conditions, in the presence and absence of Si (Fig. 3, 6th and 7th rows). With Cd and Zn, the signal was restricted to the cell corners. However, Si restored the uniform labelling in the bast fibres of plants grown with Zn and, to a lower extent, with Cd. The different signal intensity of LM16 observed may indicate a difference in the branching status of arabinan in the hypocotyl grown in the presence of Cd or Zn with Si, or also the increased activity of β-galactosidase under Cd and Zn supplementation causing loss of galactosyl residue(s) on rhamnogalacturonan I backbone to which LM16 binds (Verhertbruggen et al., 2009).

The ultrastructural analysis provided further evidence of the impact of Si, Cd and Zn on bast fibres (Fig. 3, bottom row). Under Si alone, the gelatinous G-layer (double arrow with filled tips) and fibrillar galactan-rich Gn-layer (dotted double arrow) were thicker, highlighting the role of Si in promoting cell wall deposition. Indeed, the Gn-layer (a.k.a. tertiary cell wall), which was previously detected in hemp hypocotyls aged 20 d (Behr et al., 2019), was shown to transform into the mature G-layer upon post-synthetic modifications (Chernova et al., 2018). Under Cd exposure, the bast fibres' cell wall was thicker, as previously reported using optical microscopy (Berni et al., 2024). The G-layer was indeed more developed than the control and lost its lamellar appearance, indicating a disruption of its ordered assembly; the S1-layer (thin double arrow) also became thicker, likely to compensate for the disordered structure of the G-layer. The co-treatment of Si with Cd mitigated these structural anomalies.

Under Zn exposure, the G-layer was thinner compared to C and the presence of Si alongside Zn further decreased the thickness.

The ultrastructural analysis was performed on additional tissues, namely the cambium, phloem, and xylem (Fig. 4), to obtain more detailed insights into the effects of Cd and Zn.

At the cambium level, exposure to Cd resulted in pronounced thickening of radial cell walls (Fig. 4, red arrows with filled tips) and electron-dense material also appeared. Similar electron-dense deposits were also previously reported in Cd-stressed flax hypocotyls (Douchiche et al., 2011), as well as thale cress seedlings exposed to Pb (Phang et al., 2011) and Cd-treated wheat (Moussa and El-Gamal, 2010). It remains to be determined whether such material is linked to oxidative stress.

In the presence of Si, the radial cell walls regained their original thickness, suggesting a protective or restorative role for the metalloid.

In the phloem too, Cd exposure caused an irregular swelling of the cell wall, leading to the formation of characteristic bulges along the walls (Fig. 4, red asterisks). Si stabilised the cell walls' thickness under Cd exposure.

In the xylem of control plantlets, Si induced the appearance of an S3 secondary cell wall layer (Fig. 4, thin red arrows), which can be interpreted as structural reinforcement. The addition of Cd and Zn also induced the presence of an S3 layer. Cd exposure resulted in a reduction in the thickness of the S1 and S2 secondary cell wall layers in the xylem. Remarkably, the addition of Si restored these layers to their original thickness, validating its role in preserving cellular architecture under stress. These findings emphasise the potential of Si in alleviating PTEs toxicity and maintaining the cell wall structural integrity across different cell types and tissues of the hemp hypocotyl.

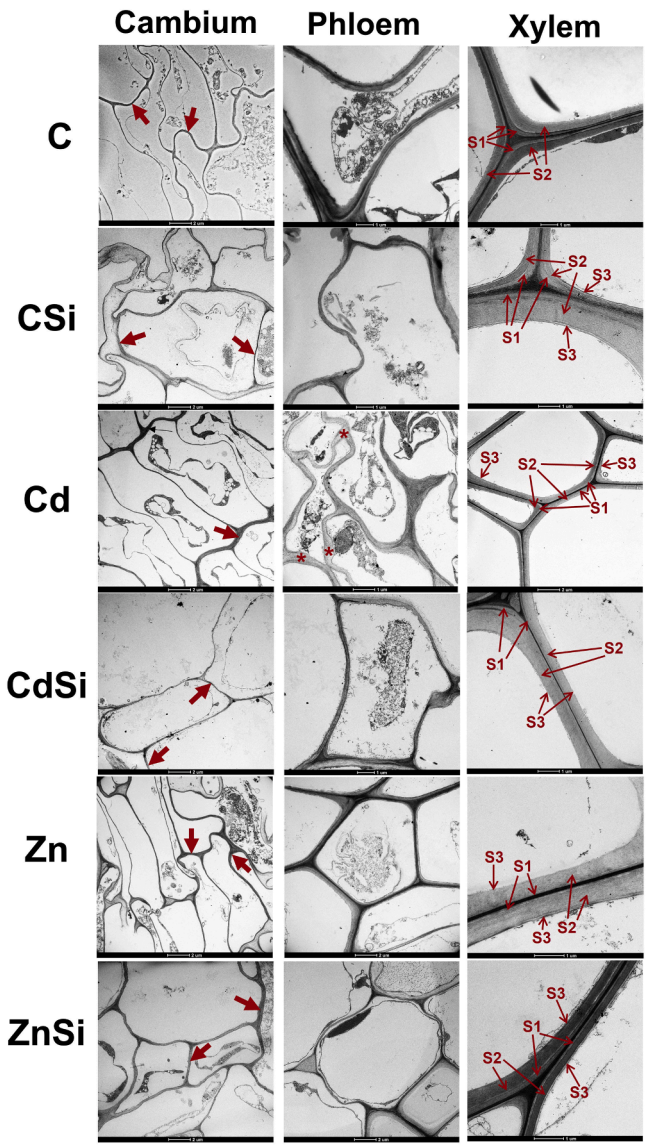

Fig. 4. Ultrastructural analysis of the cambium, phloem and xylem of hemp hypocotyls under the different treatments. The red arrows with filled tips indicate the radial cell walls; the red asterisks show bulges at the cell wall-level and the thin red arrows refer to the secondary cell wall layers S1, S2, S3. The scale bars indicate 1 or 2 μm as indicated in each panel. C: samples under control conditions, CSi: samples exposed to Si, Cd: samples exposed to Cd, CdSi: samples exposed to Cd and Si, Zn: samples exposed to Zn, ZnSi: samples exposed to Zn and Si.

3.4. *Quantification of hormones in hemp epicotyls*

Hormonomics was carried out to understand how young hemp plants regulate their response to PTEs (Fig. 5).

Among cytokinins, the metabolite *trans*-zeatin riboside (tZR), a long-distance signalling form of *trans*-zeatin (tZ) (Osugi et al., 2017), increased under ZnSi compared to Zn (Fig. 5a), suggesting a role for Si in counteracting the inhibitory effects of Zn stress by restoring cytokinin transport and signalling.

The conjugated forms of cytokinins also showed significant

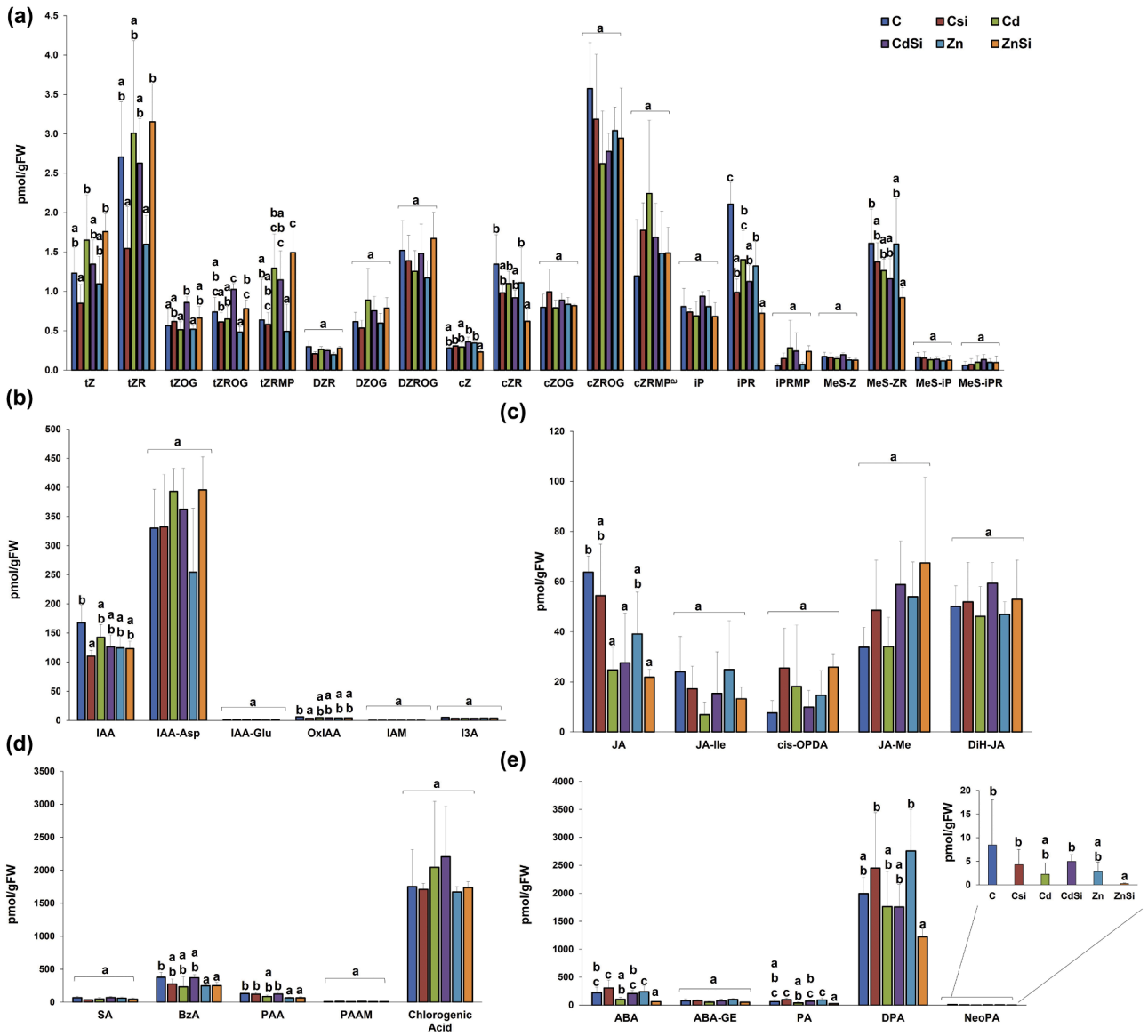

Fig. 5. Quantification of hormones in hemp epicotyls in the absence and presence of Cd, Zn and Si. Data are the means of 4 biological replicates ±SD. Different letters indicate statistically significant differences among treatments ($p<0.05$). C: samples under control conditions, CSi: samples exposed to Si, Cd: samples exposed to Cd, CdSi: samples exposed to Cd and Si, Zn: samples exposed to Zn, ZnSi: samples exposed to Zn and Si.

variations across the treatments. Notably, *trans*-zeatin-*O*-glucoside (tZOG), a glucoside conjugate of tZ playing a pivotal role in transport, storage and protection against zeatin oxidases (Martin et al., 1999), increased significantly under CdSi compared to Cd alone. This suggests that Si promoted the conjugation of tZ under Cd, likely as a mechanism to regulate the endogenous pool of cytokinins. Similarly, *trans*-zeatin riboside-*O*-glucoside (tZROG) increased significantly under both CdSi and ZnSi compared to their respective PTEs treatments alone.

Trans-zeatin riboside monophosphate (tZRMP), the precursor of tZ, increased significantly under ZnSi compared to Zn, confirming the positive impact of Si on cytokinin biosynthesis.

Under Zn, *cis*-zeatin (cZ), another zeatin isoform considered to be less active than tZ and associated to stages of limited growth such as those coinciding with the onset of a stress (Schäfer et al., 2015; Gajdosová et al., 2011), decreased under ZnSi compared to Zn, contrarily to what observed for tZ. This difference suggests a shift towards a more efficient, tZ-driven growth strategy, enabling plants to better adapt to Zn stress and benefit from Si-promoted resilience.

The riboside form of N^6-(Δ^2-isopentenyl)adenine iPR decreased significantly under CSi and Zn compared to C, reflecting suppressed transport or signalling under these conditions. Under ZnSi, iPR decreased further compared to Zn, suggesting that Si promoted a redistribution of cytokinins away from the mobile pool in response to Zn stress.

Under Si supplementation, auxin indole-3-acetic acid (IAA) levels decreased significantly compared to C (Fig. 5b). This change may reflect SiO_2-mediated reinforcement of the cell wall (Guerriero et al., 2016), which enhances structural rigidity and may consequently restrict auxin-mediated cell wall loosening and cell elongation. 2-oxoindole-3--acetic acid (Ox-IAA), a catabolic product of IAA, decreased under CSi compared to C. This reduction coincided with the decreased synthesis of IAA under CSi.

The quantification of jasmonic acid (JA) showed that Cd caused a significant decrease compared to C (Fig. 5c), suggesting that this PTE interfered with the biosynthesis/signalling pathways of JA. JA is a key hormone involved in stress responses (Hewedy et al., 2023), particularly in defence against biotic and certain abiotic stresses, but exposure to toxic levels of PTEs may impair the plant's ability to maintain JA levels

due to disruptions in enzymatic activity or precursor availability. In the literature, it was reported that JA levels increased in the leaves of Cd-stressed seedlings such as *Capsicum frutescens* (Yan et al., 2013), as well as herbaceous species (Maksymiec et al., 2005), but there is also evidence for a decrease in other species such as *Kandelia obovata* (Chen et al., 2014). These results demonstrate that the response can vary across species and may additionally depend on phenological age.

Benzoic acid (BzA) and phenylacetic acid (PAA) decreased significantly under Zn stress compared to C (Fig. 5d). This downregulation may have implications for the plant's hormonal and defence signalling network, particularly with respect to salicylic acid (SA) metabolism. BzA acts as a key intermediate in the biosynthesis of SA via the benzoate pathway; thus, its decline under Zn stress suggests a potential reduction in SA production. Since SA plays a central role in regulating redox homeostasis and mediating stress response (Saleem et al., 2021), a reduction in its precursor could decrease the plant's ability to put in place effective defence responses against stress-induced oxidative damage.

Abscisic acid (ABA) levels did not show significant changes under C and Cd exposure with/out Si, although a tendency towards lower levels could be detected upon exposure to Cd; however, with the addition of Si in the presence of Zn, ABA levels decreased significantly compared to Zn alone (Fig. 5e). This suggests that Si contributed to alleviating the stress caused by Zn, reducing the plant's reliance on ABA for stress signalling. In this respect, it is worthwhile noting that Si is known to enhance antioxidant activity in stressed plants (Kim et al., 2017).

The degradation products of ABA, i.e., phaseic acid (PA) and dihydrophaseic acid (DPA), showed a similar trend, with significant decreases in abundance under ZnSi compared to Zn alone. This reduction across ABA and its metabolites indicates that both ABA synthesis and its turnover decreased in the presence of Si under Zn stress, which supports the hypothesis of a reduced need for ABA signalling in the presence of the metalloid.

3.5. Transcriptomics of hemp hypocotyls

To shed light on the transcriptomic signature of the hemp hypocotyls grown in the different conditions, an RNA-Seq analysis was carried out. The data filtered based on FDR<0.0001 and maximum fold change (FC) in absolute value >3 resulted in 1147 differentially expressed contigs (Supplementary File 1). To visualise the data and identify clusters of genes sharing a common expression trend, a hierarchical clustering (HC) of the RNA-Seq data was performed using a Pearson correlation coefficient ≥0.61, together with a Principal Component Analysis (PCA)

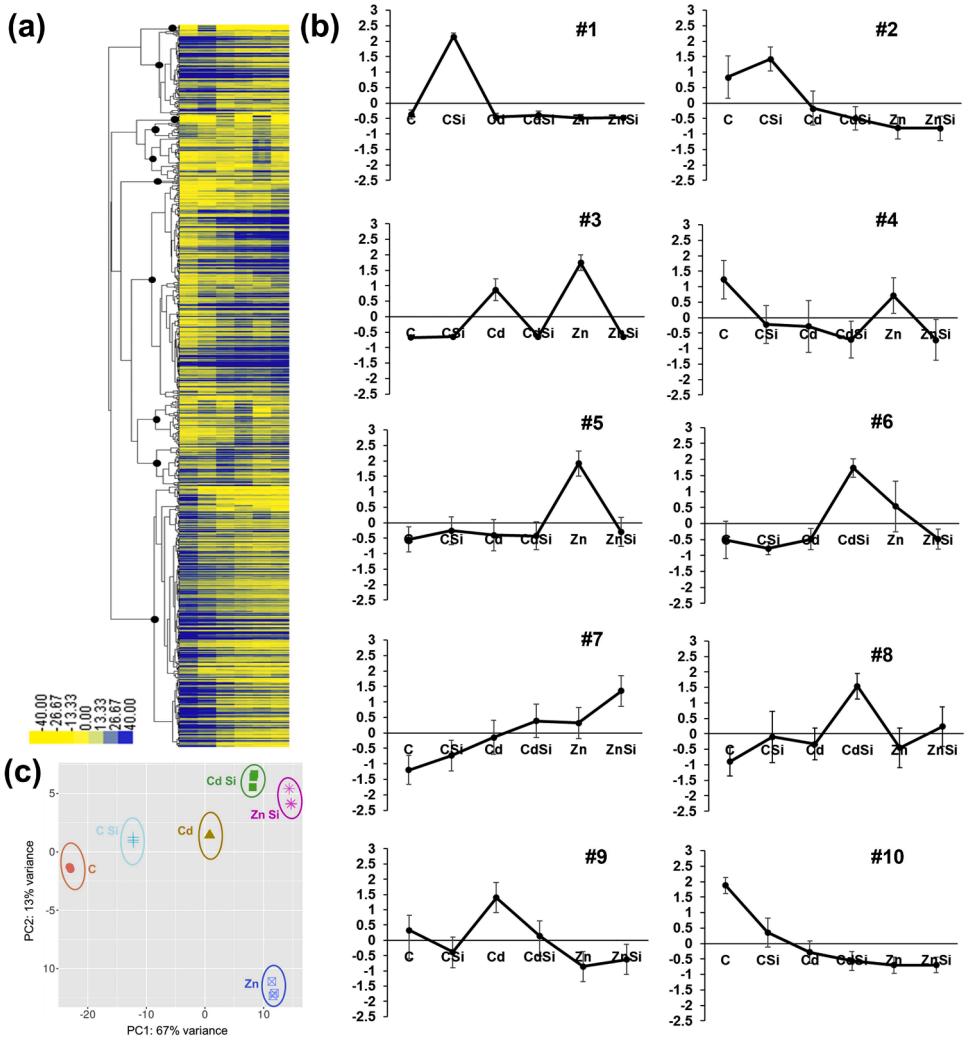

Fig. 6. Transcriptomic analysis of hemp hypocotyls grown in the absence and presence of Cd, Zn and Si. (a) Hierarchical clustering of the RNA-Seq data (black circles indicate clusters with a Pearson coefficient ≥0.61). The scale bar indicates the expression intensities. (b) Profiles of the 10 clusters showing the rescaled values ± SD (the rescaled values were obtained by subtracting the mean contig expression value of all conditions and dividing by the SD). (c) Principal Component Analysis (PCA) of the RNA-Seq data. The 6 different colours indicate the conditions. The biological replicates are enclosed in a circle. C: samples under control conditions, CSi: samples exposed to Si, Cd: samples exposed to Cd, CdSi: samples exposed to Cd and Si, Zn: samples exposed to Zn, ZnSi: samples exposed to Zn and Si.

(Fig. 6). The HC revealed the presence of 10 main expression clusters, while the PCA highlighted the presence of 6 well-separated groups corresponding to the conditions studied.

The first 2 clusters contained genes with higher expression under CSi. The 3rd cluster comprised contigs peaking under both Cd and Zn. In the 4th cluster, genes showed higher expression under C and Zn, while the 5th cluster included transcripts predominantly upregulated under Zn. The 6th and 8th clusters were characterised by contigs with higher expression under CdSi. The 7th cluster displayed a progressive increase in expression in response to PTEs exposure, reaching its maximum under ZnSi. The 9th cluster contained transcripts peaking under Cd, and the final cluster grouped genes whose expression decreased upon exposure to Si and PTEs. For each cluster, a gene ontology (GO) enrichment analysis was carried out using the default parameters in STRING (Szklarczyk et al., 2025) to elucidate the main biological processes characterising each expression pattern. Significant enrichments were found for clusters 2, 4, 7, 8 and 10 (Supplementary File 1).

3.5.1. Biological processes enriched under C and CSi

Clusters 1, 2 and 10 grouped genes expressed at higher levels in the control (C) condition, either in the absence or presence of Si. The 1st cluster did not yield a significant enrichment and grouped 7 contigs that peaked in expression in the condition CSi: contig 33800 (cysteine-rich receptor-like kinase, *CRK8*), 32031 and 33594 (corresponding to copia-like retrotransposons *At4g14460* and *At2g04490*), 14539 and 19010 (HXXXD-type acyl-transferases *At1g24430* and *AXX17_At1g25700*), 14147 (amidase *At4g34880*), 29437 (osmotin, *OSM34*). Cysteine-rich receptor-like kinases are known to play a role in stress perception, both biotic and abiotic (Wrzaczek et al., 2010). The increased expression observed under Si supplementation in the absence of PTEs indicates that Si modified the basal expression of stress-responsive genes, suggesting an altered physiological state that may influence subsequent stress responses. Additionally, the upregulation of 2 genes involved in the fatty acid metabolic process points to an enhanced suberin biosynthesis, potentially strengthening cell walls and reducing permeability under stress. Indeed, contig 14539 (FC CSi *vs* C>27) is homologous to thale cress *At1g24430* which was identified as enriched in phellem cells (Leal et al., 2022).

The induction of contig 29437 (FC CSi *vs* C=3.9), encoding the homolog of thale cress *OSM34*, further suggests activation of defence mechanisms. This protein is indeed a member of the pathogenesis-related protein PR-5 class (Anžlovar and Dermastia, 2003) which was shown to be highly expressed in *35S:ERF1* transgenic plants (Cheng et al., 2013) and to be a positive regulator of the ABA response (Park and Kim, 2021).

The hemp amidase homolog of *At4g34880* showed a FC induction under Si supplementation of 24.5: the promoter of the thale cress gene was shown to drive expression in the leaf veins with a sink-to-source pattern (Wu et al., 2013). The marked upregulation of this gene under Si treatment therefore points to a possible involvement of the metalloid in modulating vascular tissues-related functions and/or C allocation pathways.

A noteworthy finding was the upregulated expression of 2 contigs corresponding to transposable elements (copia-like and retrotransposon gag protein) under Si supplementation. This evidence may reflect Si-mediated genomic reorganisation and aligns with recent observations in barley, where Si treatment modulated DNA methylation patterns under Zn stress, suggesting that Si can influence the plant epigenome and reshape gene expression (Mazurek et al., 2025).

GO enrichment analysis of the 2nd cluster revealed biological processes related to response to stimulus, namely high light intensity, chemicals and hormones. Genes associated with photoprotection, including the hemp homologs of *A. thaliana*'s *ELIP1* (*EARLY LIGHT-INDUCED PROTEIN 1*) (Hutin et al., 2003), *CAO* (*CHLOROPLAST SIGNAL RECOGNITION PARTICLE 43*) (Klimyuk et al., 1999), *ERD7* (*EARLY-RESPONSIVE TO DEHYDRATION 7*), and *PGR5* (*PROTON GRADIENT REGULATION 5*) (Degen et al., 2024), were more highly expressed under C conditions, suggesting that the hypocotyl maintains pathways for optimal photosynthetic function and protection against excess light. Under PTEs stress, the downregulation of these genes reflects a stress-induced suppression affecting primary metabolic pathways.

The cluster also included genes involved in chemical stress responses, such as hemp homologs encoding the phytochelatin transporter ABCC1 (Song et al., 2010), as well as several transcription factors associated with abiotic stress tolerance (*DREB1A, ERF026, WRKY70*) (Sadau et al., 2024; Phukan et al., 2016), oxidative stress-related proteins (*GRXC9, OXS3*) (Herrera-Vásquez et al., 2015; Blanvillain et al., 2009) and actors of the hormone signalling pathway (*SAUR6, ABCG40*) (Borghi et al., 2015; Ren and Gray, 2015). These genes are typically associated with general stress preparedness and signalling. It is possible that these genes were activated after short-term exposure to PTEs as part of an early stress response; however, their reduced expression in 20 d-old hemp hypocotyls suggests that prolonged Cd and Zn exposure shifted the plant's physiological priorities away from general stress preparedness towards other biological processes.

Cluster 10 included the highest number of contigs (316) which were grouped in different GO terms: those including among the highest number of genes were the terms "*response to stress*", "*regulation of primary metabolic process*", "*response to oxygen-containing compounds*" and "*response to hormone*". This coordinated repression suggests a mechanism limiting energy-intensive adaptive responses to maintain basal homeostasis under adverse conditions.

In cluster 10, genes involved in cell wall-related processes were also present. Under PTEs exposure, the hypocotyl downregulated multiple components of the cell wall biosynthesis and remodelling machinery: for example, 4 contigs (2586, 8196, 16306, 27219) coding for xyloglucan endotransglucosylases/hydrolases (XETs/XTHs) were downregulated between 3- to 4-fold under Cd and 1.3- to 2-fold under Zn, 4 cellulose synthase-like transcripts (contigs 5618, 6506, 5236, 2061) decreased in expression between 2 and 3.6-fold under Cd or Zn, while 5 contigs (2769, 1222, 1950, 2467, 2574) coding for pectin lyases reached a 9.7-fold downregulation under Zn. Three of the contigs corresponding to cellulose synthase-like genes were annotated as homologs of thale cress *CSLD3*. The product of this gene was shown to be a UDP-glucose–utilising β-1,4-glucan synthase assembling into complexes with ultrastructural characteristics comparable to CESA6-containing cellulose synthase complexes (Yang et al., 2020). Such an impact on the expression of *CSLD3* homologs can in part explain the ultrastructural alterations in the bast fibre cell walls observed at the TEM (Fig. 3, bottom panels).

The impact on cellulose biosynthesis was further confirmed by the downregulation of a homolog of *A. thaliana*'s *COBL7* (*COBRA-LIKE 7*, with 4.8-fold downregulation under Zn) shown to bind cellulose and impact cellulose microfibrils' assembly (Ge et al., 2024). Similarly, the homolog of *TBL1* (*TRICHOME BIREFRINGENCE-LIKE 1*), involved in crystalline cellulose deposition (Bischoff et al., 2010), was downregulated up to 3-fold under Zn. The contig encoding the extensin-like protein EPR1 also showed downregulation up to 3.4-fold under Zn. Additionally, the reduced expression of *XET/XTH* and pectin lyase genes suggests decreased wall remodelling and loosening under PTEs; altogether, these data suggest a transition towards a more rigid cell wall architecture under PTEs.

3.5.2. Biological processes enriched under Cd and CdSi

Cluster 9 was characterised by 47 contigs peaking in expression under Cd, while clusters 6 and 8 comprised, together, 61 transcripts with highest expression under CdSi. GO enrichment was present in cluster 8 and comprised biological processes related to 2 broad categories, i.e., response to stress and organic acid catabolism.

Cd exposure is well known to trigger oxidative stress and sulphur-dependent thiol chemistry for metal chelation and vacuolar sequestration (Haider et al., 2021; Hendrix et al., 2020): the induction of *GCL1* (G

protein-coupled receptor 2-like; FC CdSi *vs* Cd=1.4), together with *DHAR1* (dehydroascorbate reductase 1; FC CdSi *vs* Cd=1.8) and the glutaredoxin *GRXS10* (FC CdSi *vs* Cd=2.2) points to the concerted reinforcement of the GSH-based redox buffering and detoxification system, enabling efficient neutralisation of ROS and formation of Cd-thiol complexes for sequestration in vacuoles and/or cell walls. This enhanced redox buffering capacity in CdSi-treated plants indicates that Si contributed to the mitigation of Cd-induced oxidative damage by strengthening antioxidant defences and promoting metal detoxification mechanisms.

Transcriptomic enrichment for organic acid catabolic process suggests that Cd and Si co-exposure triggered a reconfiguration of C metabolism in hemp hypocotyls. The induction of *PCK1* (phosphoenolpyruvate carboxykinase 1; FC CdSi *vs* Cd=3.5) and *ATBETAFRUCT4* (acid beta-fructofuranosidase 4) indicates a metabolic shift mobilising C skeletons towards organic acids and the tricarboxylic acid cycle (TCA). PCK1 catalyses indeed the cataplerotic conversion of oxaloacetate to phosphoenolpyruvate (PEP) to prevent the accumulation of TCA's intermediates and ensure cellular homeostasis (Rojas and Iglesias, 2023). The resulting PEP can then enter gluconeogenesis, or it can be further metabolised to pyruvate through glycolytic reactions. Simultaneously, the upregulation of *ATBETAFRUCT4* (FC CdSi *vs* Cd=1.4) indicates a coordinated increase in glycolytic and mitochondrial respiratory fluxes in the presence of the metalloid, supplying the ATP and reducing power needed to cope with Cd-induced stress. This combination of cataplerotic C export (via PCK1) and enhanced sucrose mobilisation (via ATBETAFRUCT4) suggests a metabolic strategy in which CdSi-treated hemp hypocotyls protect TCA-cycle integrity. By maintaining energy production and redox balance under stress conditions, these metabolic adjustments support Si-mediated protection by ensuring sufficient resources for detoxification processes and cellular repair.

The co-induction of *HPPD* (4-hydroxyphenylpyruvate dioxygenase; FC CdSi *vs* Cd=1.8) and *ISS1* (the aromatic aminotransferase *INDOLE SEVERE SENSITIVE 1*; FC CdSi *vs* Cd=2.0) delineates complementary stress responsive and aromatic amino acid-derived metabolic modules. HPPD catalyses the oxidation of 4-hydroxyphenylpyruvate to homogentisate, the key precursor of tocopherols (vitamin E), which protects cellular membranes from oxidative stress (Mishra et al., 2023). Hence, increased *HPPD* expression in the presence of Si contributes to enhanced membrane protection against Cd-induced oxidative damage.

In *Arabidopsis, ISS1* regulates tryptophan homeostasis to stabilise auxin levels: indeed, mutants lacking *ISS1* accumulate excess tryptophan and divert the flux towards tryptophan-independent auxin synthesis, highlighting its central role in preventing aromatic amino-acid overload and hormone biosynthesis dysregulation (Pieck et al., 2015). Therefore, a higher *ISS1* expression in hemp hypocotyls exposed to Cd and Si likely reflects a need for enhanced tryptophan turnover to maintain auxin balance. This regulation of auxin homeostasis may contribute to Si-mediated protection by preserving growth regulation and developmental stability under stress conditions.

The co-induction of *ELI5* (tyrosine decarboxylase; FC CdSi *vs* Cd=1.6), *PGIP1* (polygalacturonase inhibitor protein; FC CdSi *vs* Cd=2.2), and *IRX10L* (involved in xylan biosynthesis in the primary cell wall (Mortimer et al., 2015); FC CdSi *vs* Cd=3.6) in CdSi-treated hemp hypocotyls is indicative of a coordinated reinforcement and biochemical fortification of the cell wall under PTEs stress. Tyrosine decarboxylase is usually induced upon stress in plants (Facchini et al., 1999) and channels tyrosine towards tyramine, the precursor of hydroxycinnamoyl-tyramine phenolic amides, which are known to accumulate in the apoplast during abiotic stress. In parallel, the induction of *PGIP1* suggests inhibition of pectin degradation, while the upregulation of *IRX10L* indicates reinforcement of the hemicellulosic network. These transcriptional responses support a model in which Cd and Si exposure triggered a dual cell-wall defence strategy: on one hand biochemical fortification via tyramine formation and, on the other, structural strengthening through hemicellulose synthesis and inhibition of pectin degradation. Such cell wall modifications partake in Si-mediated protection by enhancing the binding and immobilisation of Cd within the apoplast, thereby limiting its cellular toxicity.

Exposure to Cd triggered a complex transcriptional reprogramming of the cell wall in hemp hypocotyls (cluster 9), as evidenced by the induction of genes involved in cell wall modification. Notably, several polygalacturonase-inhibiting proteins (*PGIP1*; contigs 21730, 22007, 26017, 29396, 33837) were induced (FC Cd *vs* C comprised between 5 and 7), suggesting reinforcement of cell wall integrity under Cd stress. Complementing this, the moderate upregulation of other cell wall-related genes (the glycoside hydrolase *CEL3*-contig 628 and *CEL1/GH9B1*-contigs 692 and 693, as well as pectin methylesterase inhibitor *PMEI*-contig 10169, expansin *EXPA4*-contig 9423, exo-polygalacturonase *PGA4*-contig 2574) with FC Cd *vs* C comprised between 1.2 and 3.5 indicates remodelling of the primary cell wall. The upregulation of the cellulases *CEL1/GH9B1* and *CEL3* together with *EXPA4* suggests activation of a wall-loosening phase, leading to the rearrangement of wall polymers and increasing the accessibility of pectin-rich domains for Cd binding. In this respect, it is interesting to note that the overexpression of *EXPA* genes was associated with increased Cd tolerance in different species (Ren et al., 2018; Zhang et al., 2018; Wang et al., 2023).

Conversely, higher *PGIP1* and *PMEI* expression suggests a subsequent cell wall stabilisation stage, in which inhibition of polygalacturonases and pectin methylesterases (PMEs) protected pectic polysaccharides from excessive depolymerisation and demethylation. These sequential remodelling and stabilisation processes indicate that Si enhanced the capacity of the cell wall to act as a dynamic structure, first increasing metal binding sites and subsequently stabilising the structure to limit Cd mobility and toxicity.

3.5.3. Biological processes enriched under Zn

Cluster 5 comprised 51 contigs that were upregulated in plants exposed to Zn and showed significant enrichment for photosynthesis-related biological processes.

Contig 1606 corresponds to the *A. thaliana* homolog of *psaA* (FC Zn *vs* C=5.9), 3 genes code for PSII components, namely *psbA* (contig 5424; FC Zn *vs* C=3.3), *psbB* (contig 10323; FC Zn *vs* C=8.0) and *psbC* (contig 2946; FC Zn *vs* C=10.7), while a fourth contig corresponds to *psbE/* cytb_{559} (contig 23561; FC Zn *vs* C=13.4). Additionally, contig 11758 is the homolog of *petB* (FC Zn *vs* C=16.5).

The genes *psaA* and *petB* encode core components of the photosynthetic electron transport chain: PsaA forms part of the PSI reaction centre, while PetB is a subunit of the cytochrome b_6/f complex that transfers electrons between PSII and I. The increased expression of *psaA* and *petB* homologs in the hemp hypocotyls reflects a compensatory response to Zn-induced oxidative stress and disruption of chloroplast redox balance to sustain photosynthetic function.

PsbB and PsbD are integral components of the PSII antenna and core reaction centre, respectively, while cytb_{559} participates in PSII assembly, contributing to secondary electron transfer and photoprotective pathways. In agreement with current understanding of chloroplast gene expression under environmental stress (Zhang et al., 2020), the observed enhanced expression of *psbB, psbD* and *psbE* in hemp indicates activation of the PSII repair and reassembly program, reflecting a chloroplast-regulated adjustment of PSII subunit production to counter Zn-induced damage.

In support of a response mechanism centred on the chloroplast, 2 contigs involved in C fixation (*rbcL* homologs, contigs 13827 and 9370 coding for RuBisCO large chain; FC Zn *vs* C>5) were up-regulated in Zn-treated plants. The up-regulation of *rbcL* preserves CO_2 assimilation and maintains C-fixation capacity. This metabolic adjustment validates previous observations in *C. sativa*: Luyckx and colleagues reported enhanced transcription of Calvin cycle and C-fixation genes in response to high Zn levels (Luyckx et al., 2021).

Under Zn stress, biological processes related to chloroplast protein

homeostasis were also observed, as demonstrated by the coordinated upregulation of plastid-encoded ribosomal protein (PRP) genes, such as *rps4, rps12*, and *rps16* (contigs 12092, 10495 and 2568; FC Zn *vs* C>4), together with increased transcription of the protease-subunit gene *clpP1* (contig 982; FC Zn *vs* C= 4.7). PRPs, long considered to possess a "housekeeping" function, were shown to play developmental and stress-responsive roles. The genetic disruption of many PRPs causes severe phenotypes including impaired chloroplast biogenesis, altered leaf morphology, compromised seedling development, as well as altered sensitivity to abiotic stresses such as cold or salinity (Robles and Quesada, 2022). Under Zn stress, the up-regulation of PRPs may reflect an increased demand to sustain synthesis of plastid-localised proteins, or to support enhanced repair and turnover of damaged plastid components.

In parallel, the induction of *clpP1* could increase proteolytic capacity within plastids, facilitating removal of misfolded or damaged proteins and maintaining plastid proteostasis.

The presence of a mechanism exerting a post-transcriptional regulation within the plastid is further supported by the upregulation of 2 contigs corresponding to the *Arabidopsis* homolog of the maturase *matK*, i.e., contigs 15405 and 17286 (FC Zn *vs* C>10). This maturase ensures efficient translation of chloroplast-encoded proteins by promoting the splicing of tRNA-K(UUU), which in turn influences the translation of plastid ribosomal proteins, thus contributing to the overall coordination of gene expression within the organelle (Muino et al., 2024). The increased expression of *matK* in hemp hypocotyls exposed to Zn indicates that the chloroplast RNA splicing capacity was boosted. Since *matK* governs the splicing of *trnK* and other group IIA introns, its upregulation suggests a shift toward safeguarding tRNA-K(UUU) production and maintaining chloroplast translation fidelity when Zn disrupts redox balance and protein homeostasis.

Mitochondrial genes involved in ATP production were also upregulated under Zn supplementation. Notably, contigs 9795 and 78 (ATP synthase α-subunit; FC Zn *vs* C>1.5), 5501 (ATP synthase β-subunit; FC Zn vs C=15), 3951 and 20574 (cyt*b* and cyt*c* oxidase subunit 1, respectively; FC Zn *vs* C>4), as well as 10649 and 9896 (NADH dehydrogenase subunit 4; FC Zn *vs* C=2.3), all showed increased expression.

Zn may interfere with electron transfer between respiratory complexes, leading to electron leakage towards O_2 and enhanced mitochondrial ROS production, a mechanism supported by a study showing that Zn-induced root cell death in rice is attenuated by inhibitors of the mitochondrial electron transport chain (Chang et al., 2005).

Cluster 5 also included molecular chaperones, such as contigs 23241 and 18857 coding for small heat shock proteins (sHSPs; FC Zn *vs* C>4), 26863 and 6078 coding, respectively, for HSP21 and chaperonin 20-CPN20 (FC Zn *vs* C>1.5). This coordinated up-regulation suggests a response to Zn-induced proteotoxic stress aimed at preserving protein homeostasis in both chloroplasts and the cytosol. HSP21 is known to associate with thylakoid membranes under stress, which supports a protective role at the photosynthetic membrane interface (Bernfur et al., 2017). The higher *CPN20* expression suggests an increased demand for ATP-dependent refolding and assembly of stromal enzymes, in line with CPN20's essential role in plastid protein folding and maintenance of plastid integrity (Zhang et al., 2025).

3.5.4. Biological processes enriched under multiple conditions

Clusters 3, 4 and 7 were characterised by contigs displaying increased expression under multiple conditions. GO term enrichment was present for clusters 4 and 7. Among the genes found in cluster 4, carbonic anhydrase-*CA* (contig 10233) displayed higher expression under control and Zn treatments but was repressed under Cd (3-fold downregulation), a pattern that reflects its central role in sustaining photosynthetic C metabolism and its sensitivity to PTEs. CA catalyses the interconversion of CO_2 and bicarbonate and, by doing so, it can help reduce the biochemical resistance to CO_2 movement within the mesophyll. In this way, CA contributes to improved CO_2 supply to the chloroplast stroma, thereby supporting more efficient photosynthetic C fixation (Momayyezi et al., 2020). Under exposure to Zn, transcript levels were comparable to the C condition; in contrast, Cd inhibited its expression, a finding suggesting a disruption of C assimilation processes and a broader repression of photosynthesis-linked pathways, consistent with Cd-induced chloroplast dysfunction and metabolic downregulation (Zulfiqar et al., 2022).

CIP1 (*COP1-interactive protein 1*; contig 6281) belongs to cluster 4 and was reported to function as a positive regulator of ABA signalling (Ren et al., 2016). In the hemp hypocotyl, it displayed a finely tuned transcriptional response across treatments that mirrored, in part, the dynamics of ABA accumulation (Fig. 5e). Under C and Zn conditions, *CIP1* levels remained comparable, in agreement with its basal role in light- and hormone-responsive signalling. *CIP1* expression declined markedly under CSi, Cd and ZnSi, suggesting that Si supplementation and/or Cd stress suppressed COP1-associated signalling pathways. However, *CIP1* was specifically upregulated under CdSi relative to Cd alone (FC CdSi *vs* Cd=2.5), indicating that Si partially reactivated this regulatory module under Cd stress. The corresponding ABA profiles reinforce this interpretation: ABA levels were stable between C and CSi, reduced under Cd, but higher under CdSi, while remaining comparable under C and Zn and declining under ZnSi. The parallel increase of *CIP1* and ABA under CdSi suggests that Si-mediated modulation of ABA signalling may restore or enhance *CIP1*-associated stress response. The absence of *CIP1* induction under ZnSi reflects the fundamentally different stress signatures of Cd and Zn. Cd strongly perturbed cellular homeostasis and suppressed ABA, allowing Si to restore ABA levels and thereby re-engage *CIP1*-dependent signalling. By contrast, Zn imposed a differently regulated stress that was not dependent on ABA in the hemp hypocotyls, and Si further reduced the perceived stress, leading to lower ABA levels under ZnSi.

The transcripts that progressively accumulated under Cd and Zn and reached maximal induction under ZnSi (cluster 7) reveal a broad reprogramming of cellular metabolism, defence, and growth regulation in hemp hypocotyls. A major component of this response involved the activation of flavonoid biosynthesis genes, i.e., *LDOX* (leucoanthocyanidin dioxygenase; contig 34419), *F3H* (flavanone 3-hydroxylase; contigs 19791 and 29196), *TT4* (*TRANSPARENT TESTA 4*; contig 12322), the homolog of *At5g42800* (dihydroflavonol 4-reductase; contig 16043) which indicate increased production of antioxidant and metal-chelating secondary metabolites. This response was further supported by the induction of triterpene biosynthetic enzymes, namely *TPS21* (*terpene synthase 21*; contig 36939), *LUP2* (*lupeol synthase 2*; contig 17859), *BAS* (*beta-amyrin synthase*; contig 11445) and *XF1* (*squalene epoxidase*; contig 6579).

The presence, in cluster 7, of multiple phytohormone network components suggests PTEs- and Si-mediated reconfiguration of several pathways. The genes comprised ethylene (*RTE1 REVERSION-TO-ETHYLENE SENSITIVITY*; contig 7839 and *EBF1 EIN3 BINDING F-BOX1*; contigs 8756 and 11575), as well as jasmonate (*JAZ3* jasmonate-zim-domain 3, *JMT* jasmonic acid carboxyl methyltransferase, *AOC4* allene oxide cyclase 4; contigs 5000, 26853, 14748, 29458), auxin (*PIN5*; contigs19934 and 27355, *PIN-LIKES 1*; contig 17627 and *PIN-LIKES 3*; contig 9767), ABA (the short-chain dehydrogenase/reductase *ABA2*; contig 19603 and *PYL4 PYR1-like 4*; contig 17559), cytokinin turnover (*CKX6*; contig 13913), and gibberellin catabolism (*GA2OX8*; contig 15838).

3.6. Proteomics of hemp hypocotyls

Gel-free proteomics was performed using a sequential protocol employing $CaCl_2$, EGTA and LiCl-complemented buffers, designed to isolate proteins with differing binding affinities for the cell wall (Printz et al., 2015). The shotgun LC-MS workflow identified 147 proteins (Supplementary File 2) that met significance criteria ($p<0.05$, maximum FC>1.5) and had a predicted extracellular localisation ≥50%. The

hierarchical clustering of the abundances revealed 7 clusters using a correlation coefficient ≥0.32 (Fig. 7). Cluster 1 and 3 were characterised by proteins peaking under ZnSi or Zn, while cluster 2 and 4 grouped proteins with increased abundance under CdSi; cluster 6 included proteins with decreased abundance under Zn, and cluster 7 proteins decreasing under PTEs, irrespective of Si presence. Cluster 5 grouped proteins with slightly higher abundance under CSi and Zn.

The focus will be hereafter put on clusters 1, 2, 3, 4, 6 and 7, given the modest increase observed in cluster 5.

3.6.1. *Proteomic signature under C and CSi*

In Cluster 7, several proteins mediating cell-wall remodelling were represented. Among those, the protein A0A7J6FHW7 showed a FC>2 when comparing CdSi or ZnSi to CSi: this protein in *C. sativa* corresponds to an activator of bc1 complex (ABC1) kinases domain and a pectin acetylesterase domain which suggests a potential role in controlling the cell wall mechanical property. It remains to be verified whether the presence of the 2 domains is an artefact due to the assembly: ABC1 kinases have been reported in plastids and mitochondria (Lundquist et al., 2012), but not in the cell wall so far.

The DUF 642-containing protein A0A7J6EHH4 is a homolog of *A. thaliana*'s AT5G11420 (FC C *vs* Zn>5) which was shown to interact with PME (Cruz-Valderrama et al., 2019; Zúñiga-Sánchez et al., 2014) and to be present in the proteome of elongating thale cress cells (Irshad et al., 2008). Other proteins involved in pectin remodelling and found at higher abundance under C condition compared to PTEs were a rhamnogalacturonase A/B/epimerase-like pectate lyase domain-containing protein (A0A7J6I2E5; FC C *vs* Zn=6), a polygalacturonase (A0A7J6EMY0; FC C *vs* Zn=3) and a PMEI domain-containing protein (A0A803NW68; FC C *vs* Zn=49). The up-regulation of a polygalacturonase and a rhamnogalacturonase/pectate-lyase–like protein supports cell wall loosening and flexibility, while the higher abundance of a PMEI indicates tight regulation of pectin de-esterification. Such a modulation maintains wall plasticity in the hypocotyls; Zn stress repressed these processes, leading to a stiffer, less extensible wall (K et al., 2025). The reduced abundance of an expansin-like A2 under PTE exposure (A0A7J6EIT0; FC C vs Zn=7) further reinforced the shift towards a stiffer cell wall state.

Among the proteins of cluster 7, it is worth noting a putative GDSL esterase-lipase (A0A803NWV7): so far, 3 GDSL esterases-lipases have been shown to be involved in cell wall patterning (Shen et al., 2022; Zhang et al., 2017; Zhang et al., 2019) and it is therefore tempting to speculate that the hemp protein might also be involved in cell wall-related processes. Its decreased abundance (ca 35-fold when comparing C *vs* Cd) suggests that Cd exposure affected pathways in which this GDSL enzyme participates.

Several peroxidases were more abundant under C condition, and many correspond to *Arabidopsis* homologs known to support hypocotyl elongation (A0A803QU24, A0A7J6HPV5) and lignification (A0A803QJ77, A0A7J6GA57, A0A803NSN1). These class III peroxidases are key modulators of wall dynamics, generating localised ROS for expansion, while also catalysing cross-linking needed to stabilise expanding walls (Cosio and Dunand, 2009). Their high abundance in C conditions reflects an active growth-related remodelling program accompanying the shift from elongation to radial growth.

3.6.2. *Proteomic signature under CdSi*

Clusters 2 and 4 grouped proteins with highest abundance under CdSi. Two fasciclin-like arabinogalactan proteins-FLAs (A0A7J6E8N8 and A0A7J6HAN1; FC CdSi *vs* CSi>8.5) were highly induced in the presence of Cd and Si: these proteins are encoded by *CsaFLA15* and *CsaFLA12*, respectively, which were highly expressed at the bottom of adult hemp stems (Guerriero et al., 2017). Cd was shown to perturb the cell wall structure and induce compensatory remodelling processes in hemp hypocotyls (Berni et al., 2024). The increased abundance of *CsaFLA12* and *CsaFLA15* reflects a wall modification program in which FLAs contributed to reorganising cellulose and matrix polysaccharides to stabilise the hypocotyl tissue under Cd. Such Si-modulated upregulation of FLAs is consistent with their established roles in controlling cell wall architecture and mechanical features (Ma et al., 2022).

The higher abundance of a procollagen-proline 4-dioxygenase (a.k.a. prolyl hydroxylase, A0A803PQP7; FC CdSi *vs* CSi=2) under CdSi confirms an intensified cell-wall remodelling response. Prolyl-4-hydroxylases hydroxylate proline residues in hydroxyproline-rich glycoproteins (HRGPs), a modification required for their proper glycosylation and cell wall structural assembly (Keskiaho et al., 2007). Cd-induced wall stress in hemp, combined with Si-mediated reinforcement, may increase the need for HRGP hydroxylation. The increased

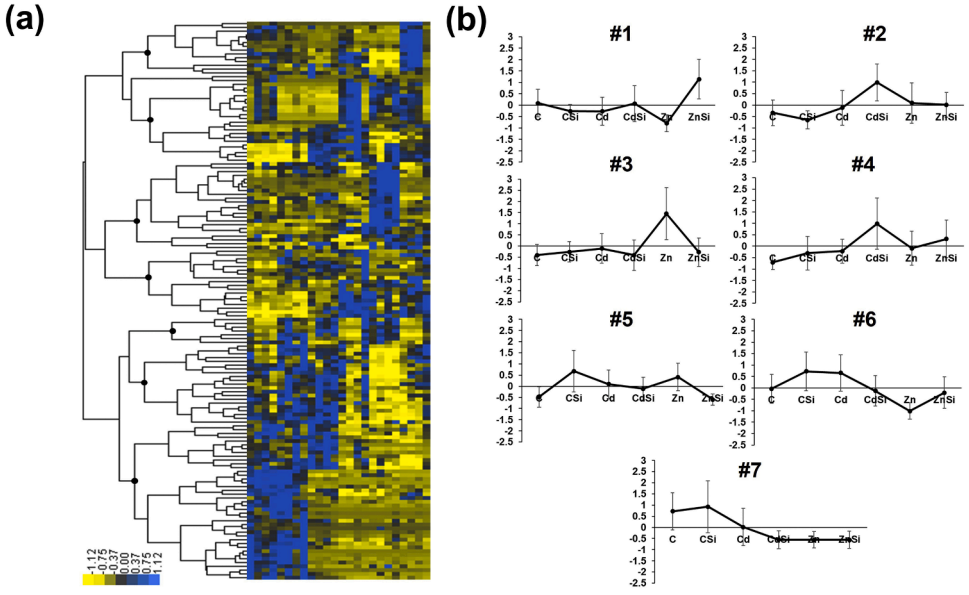

Fig. 7. Cell wall proteomic analysis of hemp hypocotyls in the absence and presence of Cd, Zn and Si. (a) Hierarchical clustering of the proteomics data (black circles indicate clusters with a Pearson coefficient ≥0.32). The scale bar indicates the abundance intensities. (b) Profiles of the 7 clusters showing the rescaled values ± SD (the rescaled values were obtained by subtracting the mean abundance value of all conditions and dividing by the SD). C: samples under control conditions, CSi: samples exposed to Si, Cd: samples exposed to Cd, CdSi: samples exposed to Cd and Si, Zn: samples exposed to Zn, ZnSi: samples exposed to Zn and Si.

P4H abundance suggests enhanced production and cross-linking of wall glycoproteins, contributing to a strengthened apoplastic barrier in the presence of Si.

In clusters 2 and 4, 7 class III peroxidases were more abundant in hemp hypocotyls grown in the presence of Cd and Si. One homologous to PRX71 (A0A7J6F7W8; FC CdSi *vs* CSi=1.4) and one to PRX35 (A0A7J6FWI6; FC CdSi *vs* CSi=1.8). Two show homology to *Arabidopsis* PRX52 (A0A7J6FET6 and A0A7J6GE89; FC CdSi *vs* CSi>5) and 2 to PRX3 (A0A7J6GI66 and A0A803QJY5; FC CdSi *vs* CSi>7), while the 4th is homologous to PRX27 (A0A803NZ20; FC CdSi *vs* CSi=345).

Noteworthy is the non-linear abundance pattern of the PRX27-like isoform, which decreased under Si alone and under Cd stress compared to C, but showed a marked induction specifically in the combined CdSi treatment. This selective activation suggests that PRX27 does not participate in Si response nor in the primary Cd-triggered peroxidase cascade but instead functions in a Si-dependent branch of the Cd-stress response. This pattern makes PRX27 a potential marker of Si-dependent modulation under PTEs in hemp.

Besides peroxidases, two PMEs (A0A7J6ENC8 with FC CdSi *vs* CSi>1000 and A0A7J6GU32 with FC CdSi *vs* CSi>3) were induced under CdSi. This result confirmed observations in pea, where Cd stress was shown to modulate PME activity to enhance Cd binding capacity in the cell wall (Gołębiowski et al., 2024).

In cluster 4, the increased abundance of a subtilisin-like protease homologous to *Arabidopsis* SBT5.3 (A0A803QB94; Fc CdSi vs CSi=2.5) suggests a role in coordinating stress responses. In *Arabidopsis*, subtilisin-like proteases showed cell type-specific expression and were responsive to JA and PTEs (Golldack et al., 2003). By analogy, SBT5.3 in hemp may contribute to activation of wall-modifying enzymes or signalling peptides in a spatially and developmentally controlled manner, supporting Cd detoxification and the restructuring of the hypocotyl cell wall under the presence of the metalloid.

Finally, the increased abundance of a RALF (Rapid Alkalinisation Factor A0A803RB93; FC CdSi *vs* CSi>13) protein under CdSi suggests activation of peptide-mediated signalling pathways. RALFs are indeed known to bind multiple receptors, triggering Ca^{2+} influx and inhibition of plasma membrane H^{+}-ATPases, which modulate apoplastic pH and downstream cell-wall dynamics (Gjetting et al., 2020). In the context of CdSi, increased RALF levels could contribute to localised pH adjustments in the cell wall, coordinating the activity of wall-modifying enzymes.

3.6.3. *Proteomic signature under Zn and ZnSi*

Within cluster 1, that grouped proteins showing high abundance under ZnSi (Supplementary File 2), the higher abundance of a glyoxal oxidase (A0A7J6DZZ7; FC ZnSi *vs* Zn=7.3) homologous to *A. thaliana*'s RUBY (Sola et al., 2019) suggests that Si co-supplementation restored enzyme levels to those observed under C conditions. Since RUBY in *Arabidopsis* functions as a putative galactose oxidase involved in pectin oxidation and modulation of cell-to-cell adhesion, it is plausible that the hemp homolog contributes similarly to cell wall remodelling and stabilisation in hypocotyl tissues. The mature hypocotyl, which has stopped elongation and entered the thickening phase, relies on well-organised pectin networks to maintain mechanical integrity and fibre cohesion. Zn stress caused a decrease in glyoxal oxidase abundance (FC C *vs* Zn=7.1), potentially compromising cell wall cross-linking, whereas Si supplementation restored its abundance to a level comparable to C. These findings align with previous observations that Si treatment preserved the fibres' properties under PTEs (Luyckx et al., 2022).

Complementing the restoration of the RUBY-like glyoxal oxidase under ZnSi, the observed increase in the abundance of a pectin acetylesterase (PAE, A0A7J6EN20; FC ZnSi *vs* Zn=3.6) suggests a Si-mediated stabilisation of pectin-modifying enzymes in the mature hemp hypocotyl. PAEs catalyse the deacetylation of pectins, a modification that directly influences cell wall stiffness, porosity and the capacity for Ca-mediated cross-linking, ultimately affecting integrity and mechanical properties. Under Zn stress, the observed decreased abundance compared to C (FC=2.9) can imply disruption of pectin architecture and weakening of the structural cohesion of the hypocotyl.

In cluster 3, the increased abundance of a knottin scorpion toxin-like domain protein (A0A7J6DU61; FC Zn *vs* C=4.9) together with an aldose 1-epimerase (A0A7J6DXN9; FC Zn *vs* C=9.8) under Zn suggests an integrated reprogramming of apoplastic defence. Knottin/defensin-like peptides are typically small, cystine-stabilised apoplastic proteins associated with antimicrobial defence and PTEs-responsive processes. The overexpression of the tobacco defensin *NtCAL1*, for instance, was shown to increase ascorbate content and the activities of key antioxidant enzymes, including catalase and ascorbate peroxidase, while simultaneously upregulating the expression of metal transport-related genes such as *NtRAMP3, NtHMAα* and *NtHMAβ* (Jin et al., 2024).

In parallel, the reported interplay between aldose 1-epimerase-like proteins (AELPs) and pectin PMEs indicates that AELP abundance can influence the degree of pectin methylesterification status, thereby regulating the density of free carboxyl groups in homogalacturonan and modulating apoplastic ion binding, wall rigidity and stress responsiveness (Sheshukova et al., 2017). In *Nicotiana*, AELP acts as part of a negative feedback loop that restrains PME activity: activation of PME during wounding or pathogen attack leads to increased methanol release, which in turn induces AELP expression. Higher abundance of AELP then suppresses *PME* gene expression at the transcriptional level, helping to return PME activity and methanol emission to baseline (Sheshukova et al., 2017). Under Zn stress, the induction of AELP may therefore serve to prevent excessive pectin demethylesterification, which could lead to excessive rigidification due to crosslinking via Ca^{2+}.

Several peptidases and proteases were also observed in cluster 3, more specifically 3 peptidase A1 domain-containing proteins (A0A7J6FVU1, A0A7J6HP45 and A0A803Q244; FC Zn *vs* C comprised between 2.6 and 5.4) and 2 subtilisin-like proteases (A0A7J6GLM7 and A0A7J6HN91; FC Zn *vs* C between 2 and 14). This is consistent with an apoplastic proteolytic response activating defence- and signalling-related precursors (peptide signals and/or cell-wall enzymes). Subtilases are well documented as secreted, cell wall-localised serine proteases that are rapidly induced by biotic and abiotic stresses and can prime immune signalling by processing extracellular substrates (Figueiredo et al., 2014). Subtilisin transcripts and activities were shown to respond to PTEs exposure (e.g., Cd) and other stresses, supporting a role for these proteases in proteome remodelling and signalling under stressful situations (Golldack et al., 2003).

Proteases and subtilases can generate or modulate mobile apoplastic signals and process cell-wall-related enzymes (Coculo et al., 2023); hence, their accumulation under Zn reflects both stress-triggered proteolysis and active remodelling/signalling aimed at stabilising the apoplast and coordinating downstream defence responses.

4. Conclusions

The integrated imaging and multi-*omics* analyses of this study demonstrated that Si acts as a key modulator of hemp resilience to Cd and Zn stress by coordinating structural, metabolic, transcriptomic and proteomic responses. By combining optical microscopy, ultrastructural analysis, hormonomics, transcriptomics and proteomics, this study established a direct link between molecular changes and functional adaptations, thereby providing a comprehensive understanding of the protective mechanism of Si under PTE stress.

At the structural level, Si preserved the organisation of bast fibre cell walls and promoted the maintenance of their ultrastructure, while molecular analyses indicated activation of cell wall-related processes and stress-responsive pathways. In parallel, Si contributed to the maintenance of cellular redox balance, energy metabolism and hormonal homeostasis, supporting plant growth and adaptation under PTE stress.

These findings support a model in which Si enhances hemp tolerance to PTEs through the coordinated reprogramming of structural and

physiological networks rather than through a single protective mechanism. Beyond providing new insights into Si biology in *C. sativa*, this work highlights the value of integrated multi-*omics* approaches to shed light on complex plant stress responses.

Funding source

This research was supported by the Luxembourg National Research Fund (INTER/FNRS/20/15045745) and by Fonds National de la Recherche Scientifique (FNRS), Belgium (convention n° T.0147.21; Application 40003569).

CRediT authorship contribution statement

Roberto Berni: Writing – review & editing, Writing – original draft, Visualization, Validation, Software, Methodology, Investigation, Formal analysis, Data curation, Conceptualization. **Céline C. Leclercq:** Writing – review & editing, Methodology, Data curation. **Sébastien Planchon:** Writing – review & editing, Methodology, Data curation. **Václav Motyka:** Writing – review & editing, Methodology, Data curation. **Petre I. Dobrev:** Writing – review & editing, Methodology, Data curation. **Sergio Sorbo:** Writing – review & editing, Methodology, Data curation. **Adriana Basile:** Writing – review & editing, Resources, Methodology, Data curation. **Jenny Renaut:** Writing – review & editing, Resources. **Stanley Lutts:** Writing – review & editing, Investigation, Funding acquisition, Conceptualization. **Gea Guerriero:** Writing – review & editing, Writing – original draft, Validation, Supervision, Resources, Project administration, Methodology, Investigation, Funding acquisition, Formal analysis, Data curation, Conceptualization.

Declaration of competing interest

The authors declare that they have no known competing financial interests or personal relationships that could have appeared to influence the work reported in this paper.

Acknowledgments

The authors are grateful to Laurent Solinhac for the assistance with the plant cultures, to Dr. Denis Pittois and Dr. Cédric Guignard for their help with the ICP-MS analyses.

Supplementary materials

Supplementary material associated with this article can be found, in the online version, at doi:10.1016/j.stress.2026.101464.

Data availability

RNA-Seq and proteomics data have been deposited in the Sequence Read Archive (SRA) under accession number PRJNA1358720 and in the PRIDE repository under dataset identifier PXD060911.

References

Akkaya, G.K., Erdal, İ, Tosun, İ, 2025. Phytoremediation potential of industrial hemp grown in sewage sludge: growth performance and environmental impact. J. Environ. Chem. Eng. 13, 117173. https://doi.org/10.1016/j.jece.2025.117173.

An, T., Gao, Y., Kuang, Q., Wu, Y., Zaman, Q uz, Zhang, Y., Xu, B., Chen, Y., 2022. Effect of silicon on morpho-physiological attributes, yield and cadmium accumulation in two maize genotypes with contrasting root system size and health risk assessment. Plant Soil 477, 117–134. https://doi.org/10.1007/s11104-022-05384-7.

Andre, C.M., Hausman, J-F, Guerriero, G., 2016. *Cannabis sativa*: the plant of the thousand and one molecules. Front. Plant Sci. 7. https://doi.org/10.3389/fpls.2016.00019.

Androudi, M., Liava, V., Tsaliki, E., Ipsilantis, I., Golia, E.E., 2024. Use of *Cannabis sativa* L. for improving cadmium-contaminated mediterranean soils—effect of mycorrhizal colonization on phytoremediation capacity. Soil. Syst. 8, 100. https://doi.org/10.3390/soilsystems8030100.

Anžlovar, S., Dermastia, M., 2003. The comparative analysis of Osmotins and Osmotin-like PR-5 proteins. Plant Biol. 5, 116–124. https://doi.org/10.1055/s-2003-40723.

Behr, M., Faleri, C., Hausman, J-F, Planchon, S., Renaut, J., Cai, G., Guerriero, G., 2019. Distribution of cell-wall polysaccharides and proteins during growth of the hemp hypocotyl. Planta 250, 1539–1556. https://doi.org/10.1007/s00425-019-03245-9.

Behr, M., Legay, S., Žižková, E., Motyka, V., Dobrev, P.I., Hausman, J-F, Lutts, S., Guerriero, G., 2016. Studying secondary growth and bast fiber development: the hemp hypocotyl peeks behind the wall. Front. Plant Sci. 7. https://doi.org/10.3389/fpls.2016.01733.

Behr, M., Lutts, S., Hausman, J-F, Sergeant, K., Legay, S., Guerriero, G., 2019. *De novo* transcriptome assembly of textile hemp from datasets on hypocotyls and adult plants. Data Brief 27. https://doi.org/10.1016/j.dib.2019.104790.

Bernfur, K., Rutsdottir, G., Emanuelsson, C., 2017. The chloroplast-localized small heat shock protein Hsp21 associates with the thylakoid membranes in heat-stressed plants. Protein Sci. 26, 1773–1784. https://doi.org/10.1002/pro.3213.

Berni, R., Hausman, J-F, Lutts, S., Guerriero, G., 2024. Histochemical and gene expression changes in *Cannabis sativa* hypocotyls exposed to increasing concentrations of cadmium and zinc. Plant Stress 14, 100668. https://doi.org/10.1016/j.stress.2024.100668.

Berni, R., Leclercq, C.C., Roux, P., Hausman, J-F, Renaut, J., Guerriero, G., 2023. A molecular study of Italian ryegrass grown on Martian regolith simulant. Sci. Total Environ. 854, 158774. https://doi.org/10.1016/j.scitotenv.2022.158774.

Berni, R., Luyckx, M., Xu, X., Legay, S., Sergeant, K., Hausman, J-F, Lutts, S., Cai, G., Guerriero, G., 2018. Reactive oxygen species and heavy metal stress in plants: Impact on the cell wall and secondary metabolism. Environ. Exp. Bot. https://doi.org/10.1016/j.envexpbot.2018.10.017.

Berni, R., Mandlik, R., Hausman, J-F, Guerriero, G., 2021. Silicon-induced mitigatory effects in salt-stressed hemp leaves. Physiol. Plant 171, 476–482. https://doi.org/10.1111/ppl.13097.

Bischoff, V., Nita, S., Neumetzler, L., Schindelasch, D., Urbain, A., Eshed, R., Persson, S., Delmer, D., Scheible, W-R, 2010. *Trichome birefringence* and its homolog *AT5G01360* encode plant-specific DUF231 proteins required for cellulose biosynthesis in arabidopsis. Plant Physiol. 153, 590–602. https://doi.org/10.1104/pp.110.153320.

Blanvillain, R., Kim, J.H., Wu, S., Lima, A., Ow, D.W., 2009. OXIDATIVE STRESS 3 is a chromatin-associated factor involved in tolerance to heavy metals and oxidative stress. Plant J. 57, 654–665. https://doi.org/10.1111/j.1365-313X.2008.03717.x.

Bokor, B., Bokorová, S., Ondoš, S., Švubová, R., Lukačová, Z., Hýblová, M., Szemes, T., Lux, A., 2015. Ionome and expression level of Si transporter genes (*Lsi1*, *Lsi2*, and *Lsi6*) affected by Zn and Si interaction in maize. Environ. Sci. Pollut. Res. Int. 22, 6800–6811. https://doi.org/10.1007/s11356-014-3876-6.

Borghi, L., Kang, J., Ko, D., Lee, Y., Martinoia, E., 2015. The role of ABCG-type ABC transporters in phytohormone transport. Biochem. Soc. Trans. 43, 924–930. https://doi.org/10.1042/BST20150106.

Bradford, M.M., 1976. A rapid and sensitive method for the quantitation of microgram quantities of protein utilizing the principle of protein-dye binding. Anal. Biochem. 72, 248–254. https://doi.org/10.1006/abio.1976.9999.

Celayir, T., Yeni, O., Yeşildirek, Y.V., Arıkan, B., Kara, N.T., 2023. Molecular Effects of Silicon on *Arabidopsis thaliana* Seedlings under UV-B Stress. Photochem. Photobiol. 99, 1393–1399. https://doi.org/10.1111/php.13788.

Chang, H-B, Lin, C-W, Huang, H-J, 2005. Zinc-induced cell death in rice (*Oryza Sativa* L.) roots. Plant Growth Regul. 46, 261–266. https://doi.org/10.1007/s10725-005-0162-0.

Chen, J., Yan, Z., Li, X., 2014. Effect of methyl jasmonate on cadmium uptake and antioxidative capacity in *Kandelia obovata* seedlings under cadmium stress. Ecotoxicol. Environ. Saf. 104, 349–356. https://doi.org/10.1016/j.ecoenv.2014.01.022.

Cheng, M-C, Liao, P-M, Kuo, W-W, Lin, T-P, 2013. The arabidopsis ETHYLENE RESPONSE FACTOR1 regulates abiotic stress-responsive gene expression by binding to different cis-acting elements in response to different stress signals. Plant Physiol. 162, 1566–1582. https://doi.org/10.1104/pp.113.221911.

Chernova, T.E., Mikshina, P.V., Salnikov, V.V., Ibragimova, N.N., Sautkina, O.V., Gorshkova, T.A., 2018. Development of distinct cell wall layers both in primary and secondary phloem fibers of hemp (*Cannabis sativa* L.). Ind. Crops. Prod. 117, 97–109. https://doi.org/10.1016/j.indcrop.2018.02.082.

Coculo, D., Del Corpo, D., Martínez, M.O., Vera, P., Piro, G., De Caroli, M., Lionetti, V., 2023. *Arabidopsis* subtilases promote defense-related pectin methylesterase activity and robust immune responses to botrytis infection. Plant Physiol. Biochem. 201, 107865. https://doi.org/10.1016/j.plaphy.2023.107865.

Cosio, C., Dunand, C., 2009. Specific functions of individual class III peroxidase genes. J. Exp. Bot. 60, 391–408. https://doi.org/10.1093/jxb/ern318.

Cruz-Valderrama, J.E., Gómez-Maqueo, X., Salazar-Iribe, A., Zúñiga-Sánchez, E., Hernández-Barrera, A., Quezada-Rodríguez, E., Gamboa-deBuen, A., 2019. Overview of the role of cell wall DUF642 proteins in plant development. Int. J. Mol. Sci. 20, 3333. https://doi.org/10.3390/ijms20133333.

Degen, G.E., Pastorelli, F., Johnson, M.P., 2024. Proton Gradient Regulation 5 is required to avoid photosynthetic oscillations during light transitions. J. Exp. Bot. 75, 947–961. https://doi.org/10.1093/jxb/erad428.

Douchiche, O., Driouich, A., Morvan, C., 2011. Impact of cadmium on early stages of flax fibre differentiation: Ultrastructural aspects and pectic features of cell walls. Plant Physiol. Biochem. 49, 592–599. https://doi.org/10.1016/j.plaphy.2011.03.008.

Eisen, M.B., Spellman, P.T., Brown, P.O., Botstein, D., 1998. Cluster analysis and display of genome-wide expression patterns. Proc. Natl. Acad. Sci. U.S.A. 95, 14863–14868.

Facchini, P.J., Yu, M., Penzes-Yost, C., 1999. Decreased cell wall digestibility in canola transformed with chimeric tyrosine decarboxylase genes from opium poppy. Plant Physiol. 120, 653–664. https://doi.org/10.1104/pp.120.3.653.

Figueiredo, A., Monteiro, F., Sebastiana, M., 2014. Subtilisin-like proteases in plant–pathogen recognition and immune priming: a perspective. Front. Plant Sci. 5. https://doi.org/10.3389/fpls.2014.00739.

Gajdosová, S., Spíchal, L., Kamínek, M., Hoyerová, K., Novák, O., Dobrev, P.I., Galuszka, P., Klíma, P., Gaudinová, A., Zizková, E., Hanus, J., Dancák, M., Trávnícek, B., Pesek, B., Krupicka, M., Vanková, R., Strnad, M., Motyka, V., 2011. Distribution, biological activities, metabolism, and the conceivable function of cis-zeatin-type cytokinins in plants. J. Exp. Bot. 62, 2827–2840. https://doi.org/10.1093/jxb/erq457.

Ge, S., Sun, P., Wu, W., Chen, X., Wang, Y., Zhang, M., Huang, J., Liang, Y-K, 2024. COBL7 is required for stomatal formation via regulation of cellulose deposition in *Arabidopsis*. New Phytol. 241, 227–242. https://doi.org/10.1111/nph.19327.

Gjetting, S.K., Mahmood, K., Shabala, L., Kristensen, A., Shabala, S., Palmgren, M., Fuglsang, A.T., 2020. Evidence for multiple receptors mediating RALF-triggered Ca2 + signaling and proton pump inhibition. Plant J. 104, 433–446. https://doi.org/10.1111/tpj.14935.

Gołębiowski, A., Szultka-Młyńska, M., Pomastowski, P., Rafińska, K., Orzoł, A., Cichorek, M., Olszewski, J., Buszewski, B., Głowacka, K., 2024. Role of silicon in counteracting cadmium stress in pea plants (*Pisum sativum* L.): insights into cadmium binding mechanisms and pectin methylesterase activity. J. Soil. Sci. Plant Nutr. 24, 5613–5625. https://doi.org/10.1007/s42729-024-01929-0.

Golldack, D., Vera, P., Dietz, K-J, 2003. Expression of subtilisin-like serine proteases in *Arabidopsis thaliana* is cell-specific and responds to jasmonic acid and heavy metals with developmental differences. Physiol. Plant 118, 64–73. https://doi.org/10.1034/j.1399-3054.2003.00087.x.

Guerriero, G., Achen, C., Xu, X., Planchon, S., Leclercq, C.C., Sergeant, K., Berni, R., Hausman, J-F, Renaut, J., Legay, S., 2021. The cell wall proteome of *Craterostigma plantagineum* cell cultures habituated to dichlobenil and isoxaben. Cells 10, 2295. https://doi.org/10.3390/cells10092295.

Guerriero, G., Deshmukh, R., Sonah, H., Sergeant, K., Hausman, J-F, Lentzen, E., Valle, N., Siddiqui, K.S., Exley, C., 2019. Identification of the aquaporin gene family in *Cannabis sativa* and evidence for the accumulation of silicon in its tissues. Plant Sci. 287, 110167. https://doi.org/10.1016/j.plantsci.2019.110167.

Guerriero, G., Hausman, J-F, Legay, S., 2016. Silicon and the plant extracellular matrix. Front. Plant Sci. 7. https://doi.org/10.3389/fpls.2016.00463.

Guerriero, G., Mangeot-Peter, L., Legay, S., Behr, M., Lutts, S., Siddiqui, K.S., Hausman, J-F, 2017. Identification of fasciclin-like arabinogalactan proteins in textile hemp (*Cannabis sativa* L.): in silico analyses and gene expression patterns in different tissues. BMC Genomics 18. https://doi.org/10.1186/s12864-017-3970-5.

Haider, F.U., Liqun, C., Coulter, J.A., Cheema, S.A., Wu, J., Zhang, R., Wenjun, M., Farooq, M., 2021. Cadmium toxicity in plants: impacts and remediation strategies. Ecotoxicol. Environ. Saf. 211, 111887. https://doi.org/10.1016/j.ecoenv.2020.111887.

Hendrix, S., Jozefczak, M., Wójcik, M., Deckers, J., Vangronsveld, J., Cuypers, A., 2020. Glutathione: a key player in metal chelation, nutrient homeostasis, cell cycle regulation and the DNA damage response in cadmium-exposed *Arabidopsis thaliana*. Plant Physiol. Biochem. 154, 498–507. https://doi.org/10.1016/j.plaphy.2020.06.006.

Herrera-Vásquez, A., Carvallo, L., Blanco, F., Tobar, M., Villarroel-Candia, E., Vicente-Carbajosa, J., Salinas, P., Holuigue, L., 2015. Transcriptional control of glutaredoxin GRXC9 expression by a salicylic acid-dependent and npr1-independent pathway in *Arabidopsis*. Plant Mol. Biol. Rep. 33, 624–637. https://doi.org/10.1007/s11105-014-0782-5.

Hewedy, O.A., Elsheery, N.I., Karkour, A.M., Elhamouly, N., Arafa, R.A., Mahmoud, GA-E, Dawood, MF-A, Hussein, W.E., Mansour, A., Amin, D.H., Allakhverdiev, S.I., Zivcak, M., Brestic, M., 2023. Jasmonic acid regulates plant development and orchestrates stress response during tough times. Environ. Exp. Bot. 208, 105260. https://doi.org/10.1016/j.envexpbot.2023.105260.

Huang, L., Li, H., Luo, Y., Shi, J., Kong, L., Teng, W., 2024. Exogenous silicon alleviates aluminum stress in *Eucalyptus* species by enhancing the antioxidant capacity and improving plant growth and tolerance quality. BMC Plant Biol. 24, 997. https://doi.org/10.1186/s12870-024-05723-z.

Huang, W., Zhang, C., Zhu, B., Liu, X., Xiao, H., Liu, S., Shao, H., 2025. Systematic evaluation of plant metals/metalloids accumulation efficiency: a global synthesis of bioaccumulation and translocation factors. Front. Plant Sci. 16, 1602951. https://doi.org/10.3389/fpls.2025.1602951.

Hutin, C., Nussaume, L., Moise, N., Moya, I., Kloppstech, K., Havaux, M., 2003. Early light-induced proteins protect *Arabidopsis* from photooxidative stress. Proc. Natl. Acad. Sci. U.S.A. 100, 4921–4926. https://doi.org/10.1073/pnas.0736939100.

Irshad, M., Canut, H., Borderies, G., Pont-Lezica, R., Jamet, E., 2008. A new picture of cell wall protein dynamics in elongating cells of *Arabidopsis thaliana*: confirmed actors and newcomers. BMC Plant Biol. 8, 94. https://doi.org/10.1186/1471-2229-8-94.

Jin, W., Wang, H., Liu, Q., Deng, Z., Li, X., Xu, X., Hao, H., Wu, S., Shi, Y., Guo, H., 2024. The defensin protein NtCAL1 functions as a positive factor in plant cadmium accumulation and resistance in tobacco. Environ. Exp. Bot. 225, 105866. https://doi.org/10.1016/j.envexpbot.2024.105866.

K, S A, Puthur, J.T., Dhankher, O.P., 2025. Plant cell wall remodeling under toxic metal stress: structural adaptation and functional implications. Environ. Sci. Technol. 59, 21386–21400. https://doi.org/10.1021/acs.est.5c05890.

Keskiaho, K., Hieta, R., Sormunen, R., Myllyharju, J., 2007. *Chlamydomonas reinhardtii* has multiple prolyl 4-hydroxylases, one of which is essential for proper cell wall assembly. Plant Cell 19, 256–269. https://doi.org/10.1105/tpc.106.042739.

Kim, Y-H, Khan, A.L., Waqas, M., Lee, I-J, 2017. Silicon regulates antioxidant activities of crop plants under abiotic-induced oxidative stress: a review. Front. Plant Sci. 8. https://doi.org/10.3389/fpls.2017.00510.

Klimyuk, V.I., Persello-Cartieaux, F., Havaux, M., Contard-David, P., Schuenemann, D., Meiherhoff, K., Gouet, P., Jones, J.D.G., Hoffman, N.E., Nussaume, L., 1999. A chromodomain protein encoded by the *Arabidopsis CAO* gene is a plant-specific component of the chloroplast signal recognition particle pathway that is involved in LHCP targeting. Plant Cell 11, 87–99. https://doi.org/10.1105/tpc.11.1.87.

Lavanya, M.B., Viswanath, D.S., Sivapullaiah, P.V., 2024. Phytoremediation: an eco-friendly approach for remediation of heavy metal-contaminated soils-a comprehensive review. Environ. Nanotechnol. Monit. Manage. 22, 100975. https://doi.org/10.1016/j.enmm.2024.100975.

Leal, A.R., Barros, P.M., Parizot, B., Sapeta, H., Vangheluwe, N., Andersen, T.G., Beeckman, T., Oliveira, M.M., 2022. Translational profile of developing phellem cells in *Arabidopsis thaliana* roots. Plant J. 110, 899–915. https://doi.org/10.1111/tpj.15691.

Lin, Y-F, Aarts, M.G.M., 2012. The molecular mechanism of zinc and cadmium stress response in plants. Cell Mol. Life Sci. 69, 3187–3206. https://doi.org/10.1007/s00018-012-1089-z.

Lundquist, P.K., Davis, J.I., van Wijk, K.J., 2012. ABC1K atypical kinases in plants; filling the organellar kinase void. Trends Plant Sci. 17, 546–555. https://doi.org/10.1016/j.tplants.2012.05.010.

Luyckx, M., Blanquet, M., Isenborghs, A., Guerriero, G., Bidar, G., Waterlot, C., Douay, F., Lutts, S., 2022. Impact of silicon and heavy metals on hemp (*Cannabis sativa* L.) bast fibres properties: an industrial and agricultural perspective. Int. J. Environ. Res. 16, 82. https://doi.org/10.1007/s41742-022-00446-1.

Luyckx, M., Hausman, J-F, Blanquet, M., Guerriero, G., Lutts, S., 2021. Silicon reduces cadmium absorption and increases root-to-shoot translocation without impacting growth in young plants of hemp (*Cannabis sativa* L.) on a short-term basis. Environ. Sci. Pollut. Res. Int. 28, 37963–37977. https://doi.org/10.1007/s11356-021-12912-y.

Luyckx, M., Hausman, J-F, Guerriero, G., Lutts, S., 2023. Silicon reduces zinc absorption and triggers oxidative tolerance processes without impacting growth in young plants of hemp (*Cannabis sativa* L.). Environ. Sci. Pollut. Res. Int. 30, 943–955. https://doi.org/10.1007/s11356-022-21797-4.

Luyckx, M., Hausman, J-F, Isenborghs, A., Guerriero, G., Lutts, S., 2021. Impact of cadmium and zinc on proteins and cell wall-related gene expression in young stems of hemp (*Cannabis sativa* L.) and influence of exogenous silicon. Environ. Exp. Bot. 183, 104363. https://doi.org/10.1016/j.envexpbot.2020.104363.

Luyckx, M., Hausman, J-F, Sergeant, K., Guerriero, G., Lutts, S., 2021. Molecular and biochemical insights into early responses of hemp to Cd and Zn exposure and the potential effect of Si on stress response. Front. Plant Sci. 12, 711853. https://doi.org/10.3389/fpls.2021.711853.

Ma, Y., MacMillan, C.P., de Vries, L., Mansfield, S.D., Hao, P., Ratcliffe, J., Bacic, A., Johnson, K.L., 2022. FLA11 and FLA12 glycoproteins fine-tune stem secondary wall properties in response to mechanical stresses. New. Phytol. 233, 1750–1767. https://doi.org/10.1111/nph.17898.

Maksymiec, W., Wianowska, D., Dawidowicz, A.L., Radkiewicz, S., Mardarowicz, M., Krupa, Z., 2005. The level of jasmonic acid in *Arabidopsis thaliana* and *Phaseolus coccineus* plants under heavy metal stress. J. Plant Physiol. 162, 1338–1346. https://doi.org/10.1016/j.jplph.2005.01.013.

Manivannan, A., Soundararajan, P., Jeong, B.R., 2023. Editorial: silicon: a "quasi-essential" element's role in plant physiology and development. Front. Plant Sci. 14. https://doi.org/10.3389/fpls.2023.1157185.

Marabesi, A.O., Nambeesan, S.U., van Iersel, M.W., Lessl, J.T., Coolong, T.W., 2023. Cadmium exposure is associated with increased transcript abundance of multiple heavy metal associated transporter genes in roots of hemp (*Cannabis sativa* L.). Front. Plant Sci. 14. https://doi.org/10.3389/fpls.2023.1183249.

Marabesi, A.O., Nambeesan, S.U., van Iersel, M.W., Lessl, J.T., Coolong, T.W., 2023. Cadmium exposure is associated with increased transcript abundance of multiple heavy metal associated transporter genes in roots of hemp (*Cannabis sativa* L.). Front. Plant Sci. 14. https://doi.org/10.3389/fpls.2023.1183249.

Maresca, V., Teta, R., Finamore, C., Cianciullo, P., Sorbo, S., D'Auria, M.V., Basile, A., 2023. Heavy metal stress induces adaptative responses in the liverwort *Conocephalum conicum* L. (Dum.): an integrated biologic and metabolomic study. Environ. Exp. Bot. 209, 105292. https://doi.org/10.1016/j.envexpbot.2023.105292.

Martin, R.C., Mok, M.C., Mok, D.W.S., 1999. Isolation of a cytokinin gene, ZOG1, encoding zeatin O-glucosyltransferase from *Phaseolus lunatus*. Proc. Natl. Acad. Sci. U.S.A. 96, 284–289. https://doi.org/10.1073/pnas.96.1.284.

Mazurek, M., Tobiasz-Salach, R., Stadnik, B., Migut, D., 2025. Silicon-mitigated effect on zinc-induced stress conditions: epigenetic, morphological, and physiological screening of barley plants. Int. J. Mol. Sci. 26, 104. https://doi.org/10.3390/ijms26010104.

Meng, Y., Xiang, C., Huo, J., Shen, S., Tang, Y., Wu, L., 2023. Toxicity effects of zinc supply on growth revealed by physiological and transcriptomic evidences in sweet potato (*Ipomoea batatas* (L.) Lam). Sci. Rep. 13, 19203. https://doi.org/10.1038/s41598-023-46504-2.

Mishra, N., Jiang, C., Chen, L., Paul, A., Chatterjee, A., Shen, G., 2023. Achieving abiotic stress tolerance in plants through antioxidative defense mechanisms. Front. Plant Sci. 14. https://doi.org/10.3389/fpls.2023.1110622.

Mišúthová, A., Slováková, Ľ, Kollárová, K., Vaculík, M., 2021. Effect of silicon on root growth, ionomics and antioxidant performance of maize roots exposed to as toxicity. Plant Physiol. Biochem. 168, 155–166. https://doi.org/10.1016/j.plaphy.2021.10.012.

Momayyezi, M., McKown, A.D., Bell, S.C.S., Guy, R.D., 2020. Emerging roles for carbonic anhydrase in mesophyll conductance and photosynthesis. Plant J. 101, 831–844. https://doi.org/10.1111/tpj.14638.

Mortimer, J.C., Faria-Blanc, N., Yu, X., Tryfona, T., Sorieul, M., Ng, Y.Z., Zhang, Z., Stott, K., Anders, N., Dupree, P., 2015. An unusual xylan in *Arabidopsis* primary cell

walls is synthesised by GUX3, IRX9L, IRX10L and IRX14. Plant J. 83, 413–426. https://doi.org/10.1111/tpj.12898.
Motrescu, I., Luchian, C.E., 2026. Bioremediation of heavy metal-contaminated agricultural soils: mechanisms, emerging technologies, and pathways to field-scale application. Agriculture 16, 1215. https://doi.org/10.3390/agriculture16111215.
Moussa, H.R., El-Gamal, S.M., 2010. Effect of salicylic acid pretreatment on cadmium toxicity in wheat. Biologia Plantarum 54, 315–320. https://doi.org/10.1007/s10535-010-0054-7.
Muino, J.M., Ruwe, H., Qu, Y., Maschmann, S., Chen, W., Zoschke, R., Ohler, U., Kaufmann, K., Schmitz-Linneweber, C., 2024. MatK impacts differential chloroplast translation by limiting spliced tRNA-K(UUU) abundance. Plant J. 119, 2737–2752. https://doi.org/10.1111/tpj.16945.
Nash, A.O.M., Joshee, N., Sherman, S., Lessl, J.T., Coolong, T., 2024. Accumulation and histochemical localization of cadmium in hemp (*Cannabis sativa* L.) leaf and root tissue. HortScience 59, 1150–1157. https://doi.org/10.21273/HORTSCI17930-24.
Ondrasek, G., Shepherd, J., Rathod, S., Dharavath, R., Imtiaz Rashid, M., Brtnicky, M., Shafiq Shahid, M., Horvatinec, J., Rengel, Z., 2025. Metal contamination – a global environmental issue: sources, implications & advances in mitigation. RSC Adv. 15, 3904–3927. https://doi.org/10.1039/D4RA04639K.
Osugi, A., Kojima, M., Takebayashi, Y., Ueda, N., Kiba, T., Sakakibara, H., 2017. Systemic transport of *trans*-zeatin and its precursor have differing roles in *Arabidopsis* shoots. Nat. Plants 3, 17112. https://doi.org/10.1038/nplants.2017.112.
Park, E-J, Kim, T-H, 2021. Arabidopsis OSMOTIN 34 functions in the ABA signaling pathway and is regulated by proteolysis. Int. J. Mol. Sci. 22, 7915. https://doi.org/10.3390/ijms22157915.
Phang, I.C., Leung, D.W.M., Taylor, H.H., Burritt, D.J., 2011. Correlation of growth inhibition with accumulation of Pb in cell wall and changes in response to oxidative stress in *Arabidopsis thaliana* seedlings. Plant Growth Regul. 64, 17–25. https://doi.org/10.1007/s10725-010-9527-0.
Phukan, U.J., Jeena, G.S., Shukla, R.K., 2016. WRKY transcription factors: molecular regulation and stress responses in plants. Front. Plant Sci. 7. https://doi.org/10.3389/fpls.2016.00760.
Pieck, M., Yuan, Y., Godfrey, J., Fisher, C., Zolj, S., Vaughan, D., Thomas, N., Wu, C., Ramos, J., Lee, N., Normanly, J., Celenza, J.L., 2015. Auxin and tryptophan homeostasis are facilitated by the ISS1/VAS1 aromatic aminotransferase in *Arabidopsis*. Genetics 201, 185–199. https://doi.org/10.1534/genetics.115.180356.
Printz, B., Dos Santos Morais, R., Wienkoop, S., Sergeant, K., Lutts, S., Hausman, J-F, Renaut, J., 2015. An improved protocol to study the plant cell wall proteome. Front. Plant Sci. 6. https://doi.org/10.3389/fpls.2015.00237.
Rasin, P., V, A.A., Basheer, S.M., Haribabu, J., Santibanez, J.F., Garrote, C.A., Arulraj, A., Mangalaraja, R.V., 2025. Exposure to cadmium and its impacts on human health: a short review. J. Hazard. Mater. Adv. 17, 100608. https://doi.org/10.1016/j.hazadv.2025.100608.
Ren, C., Zhu, X., Zhang, P., Gong, Q., 2016. Arabidopsis COP1-interacting protein 1 is a positive regulator of ABA response. Biochem. Biophys. Res. Commun. 477, 847–853. https://doi.org/10.1016/j.bbrc.2016.06.147.
Ren, H., Gray, W.M., 2015. SAUR proteins as effectors of hormonal and environmental signals in plant growth. Mol. Plant 8, 1153–1164. https://doi.org/10.1016/j.molp.2015.05.003.
Ren, Y., Chen, Y., An, J., Zhao, Z., Zhang, G., Wang, Y., Wang, W., 2018. Wheat expansin gene *TaEXPA2* is involved in conferring plant tolerance to Cd toxicity. Plant Sci. 270, 245–256. https://doi.org/10.1016/j.plantsci.2018.02.022.
Robles, P., Quesada, V., 2022. Unveiling the functions of plastid ribosomal proteins in plant development and abiotic stress tolerance. Plant Physiol. Biochem. 189, 35–45. https://doi.org/10.1016/j.plaphy.2022.07.029.
Rojas, B.E., Iglesias, A.A., 2023. Integrating multiple regulations on enzyme activity: the case of phosphoenolpyruvate carboxykinases. AoB Plants 15, plad053. https://doi.org/10.1093/aobpla/plad053.
Sadau, S.B., Liu, Z., Ninkuu, V., Guan, L., Sun, X., 2024. DREB transcription factors are crucial regulators of abiotic stress responses in *Gossypium* spp. Plant Stress 11, 100350. https://doi.org/10.1016/j.stress.2024.100350.
Saldanha, A.J., 2004. Java Treeview–extensible visualization of microarray data. Bioinformatics 20, 3246–3248. https://doi.org/10.1093/bioinformatics/bth349.
Saleem, M., Fariduddin, Q., Castroverde, C.D.M., 2021. Salicylic acid: a key regulator of redox signalling and plant immunity. Plant Physiol. Biochem. 168, 381–397. https://doi.org/10.1016/j.plaphy.2021.10.011.
Schäfer, M., Brütting, C., Canales, I.M., Großkinsky, D.K., Vankova, R., Baldwin, I.T., Meldau, S., 2015. The role of cis-zeatin-type cytokinins in plant growth regulation and mediating responses to environmental interactions. J. Exp. Bot. 66, 4873–4884. https://doi.org/10.1093/jxb/erv214.
Schmidt, V., Skokan, R., Depaepe, T., Kurtović, K., Haluška, S., Vosolsobě, S., Vaculíková, R., Pil, A., Dobrev, P.I., Motyka, V., Van Der Straeten, D., Petrášek, J., 2024. Phytohormone profiling in an evolutionary framework. Nat. Commun. 15, 3875. https://doi.org/10.1038/s41467-024-47753-z.
Shen, G., Sun, W., Chen, Z., Shi, L., Hong, J., Shi, J., 2022. Plant GDSL esterases/lipases: evolutionary, physiological and molecular functions in plant development. Plants 11, 468. https://doi.org/10.3390/plants11040468.
Shen, Z., Pu, X., Wang, S., Dong, X., Cheng, X., Cheng, M., 2022. Silicon improves ion homeostasis and growth of liquorice under salt stress by reducing plant Na+ uptake. Sci. Rep. 12, 5089. https://doi.org/10.1038/s41598-022-09061-8.
Sheshukova, E.V., Komarova, T.V., Pozdyshev, D.V., Ershova, N.M., Shindyapina, A.V., Tashlitsky, V.N., Sheval, E.V., Dorokhov, Y.L., 2017. The intergenic interplay between aldose 1-epimerase-like protein and pectin methylesterase in abiotic and biotic stress control. Front. Plant Sci. 8. https://doi.org/10.3389/fpls.2017.01646.
Šola, K., Gilchrist, E.J., Ropartz, D., Wang, L., Feussner, I., Mansfield, S.D., Ralet, M-C, Haughn, G.W., 2019. RUBY, a putative galactose oxidase, influences pectin properties and promotes cell-to-cell adhesion in the seed coat epidermis of *Arabidopsis*. Plant Cell 31, 809–831. https://doi.org/10.1105/tpc.18.00954.
Song, J., Yang, J., Jeong, B.R., 2024. Synergistic effects of silicon and aspartic acid on the alleviation of salt stress in celery (*Apium graveliens* L.) "Si Ji Xiao Xiang Qin.". Plants 13, 2072. https://doi.org/10.3390/plants13152072.
Song, W-Y, Park, J., Mendoza-Cózatl, D.G., Suter-Grotemeyer, M., Shim, D., Hörtensteiner, S., Geisler, M., Weder, B., Rea, P.A., Rentsch, D., Schroeder, J.I., Lee, Y., Martinoia, E., 2010. Arsenic tolerance in *Arabidopsis* is mediated by two ABCC-type phytochelatin transporters. Proc. Natl. Acad. Sci. U.S.A. 107, 21187–21192. https://doi.org/10.1073/pnas.1013964107.
Soni, S., Jha, A.B., Dubey, R.S., Sharma, P., 2024. Mitigating cadmium accumulation and toxicity in plants: the promising role of nanoparticles. Sci. Total Environ. 912, 168826. https://doi.org/10.1016/j.scitotenv.2023.168826.
Szklarczyk, D., Nastou, K., Koutrouli, M., Kirsch, R., Mehryary, F., Hachilif, R., Hu, D., Peluso, M.E., Huang, Q., Fang, T., Doncheva, N.T., Pyysalo, S., Bork, P., Jensen, L.J., von Mering, C., 2025. The STRING database in 2025: protein networks with directionality of regulation. Nucleic Acids Res. 53, D730–D737. https://doi.org/10.1093/nar/gkae1113.
Thumuluri, V., Almagro Armenteros, J.J., Johansen, A.R., Nielsen, H., Winther, O., 2022. DeepLoc 2.0: multi-label subcellular localization prediction using protein language models. Nucleic Acids Res. 50, W228–W234. https://doi.org/10.1093/nar/gkac278.
Van, H-T, Hoang, V.H., Nga, L.T.Q., Nguyen, V.Q., 2024. Effects of Zn pollution on soil: pollution sources, impacts and solutions. Results Surf. Interfaces 17, 100360. https://doi.org/10.1016/j.rsurfi.2024.100360.
Verhertbruggen, Y., Marcus, S.E., Haeger, A., Verhoef, R., Schols, H.A., McCleary, B.V., McKee, L., Gilbert, H.J., Paul Knox, J., 2009. Developmental complexity of arabinan polysaccharides and their processing in plant cell walls. Plant J. 59, 413–425. https://doi.org/10.1111/j.1365-313X.2009.03876.x.
Vizcaíno, J.A., Csordas, A., del-Toro, N., Dianes, J.A., Griss, J., Lavidas, I., Mayer, G., Perez-Riverol, Y., Reisinger, F., Ternent, T., Xu, Q-W, Wang, R., Hermjakob, H., 2016. 2016 update of the PRIDE database and its related tools. Nucleic Acids Res. 44, D447–D456. https://doi.org/10.1093/nar/gkv1145.
Wang, H., Yu, J., Zhu, B., Gu, L., Wang, H., Du, X., Zeng, T., Tang, H., 2023. The SbbHLH041–SbEXPA11 module enhances cadmium accumulation and rescues biomass by increasing photosynthetic efficiency in sorghum. Int. J. Mol. Sci. 24, 13061. https://doi.org/10.3390/ijms241713061.
Wrzaczek, M., Brosché, M., Salojärvi, J., Kangasjärvi, S., Idänheimo, N., Mersmann, S., Robatzek, S., Karpiński, S., Karpińska, B., Kangasjärvi, J., 2010. Transcriptional regulation of the CRK/DUF26 group of receptor-like protein kinases by ozone and plant hormones in *Arabidopsis*. BMC Plant Biol. 10, 95. https://doi.org/10.1186/1471-2229-10-95.
Wu, X., Huang, R., Liu, Z., Zhang, G., 2013. Functional characterization of cis-elements conferring vascular vein expression of At4g34880 amidase family protein gene in *Arabidopsis*. PLoS One 8, e67562. https://doi.org/10.1371/journal.pone.0067562.
Xu, X., Guerriero, G., Domergue, F., Beine-Golovchuk, O., Cocco, E., Berni, R., Sergeant, K., Hausman, J-F, Legay, S., 2023. Characterization of MdMYB68, a suberin master regulator in russeted apples. Front. Plant Sci. 14. https://doi.org/10.3389/fpls.2023.1143961.
Yan, Z., Chen, J., Li, X., 2013. Methyl jasmonate as modulator of Cd toxicity in *Capsicum frutescens* var. fasciculatum seedlings. Ecotoxicol. Environ. Saf. 98, 203–209. https://doi.org/10.1016/j.ecoenv.2013.08.019.
Yang, J., Bak, G., Burgin, T., Barnes, W.J., Mayes, H.B., Peña, M.J., Urbanowicz, B.R., Nielsen, E., 2020. Biochemical and genetic analysis identify CSLD3 as a beta-1,4-glucan synthase that functions during plant cell wall synthesis. Plant Cell 32, 1749–1767. https://doi.org/10.1105/tpc.19.00637.
Yang, J., Song, J., Jeong, B.R., 2022. Drenched silicon suppresses disease and insect pests in coffee plant grown in controlled environment by improving physiology and upregulating defense genes. Int. J. Mol. Sci. 23, 3543. https://doi.org/10.3390/ijms23073543.
Zhang, B., Zhang, L., Li, F., Zhang, D., Liu, X., Wang, H., Xu, Z., Chu, C., Zhou, Y., 2017. Control of secondary cell wall patterning involves xylan deacetylation by a GDSL esterase. Nat. Plants 3, 17017. https://doi.org/10.1038/nplants.2017.17.
Zhang, H., Ding, Y., Zhi, J., Li, X., Liu, H., Xu, J., 2018. Over-expression of the poplar expansin gene *PtoEXPA12* in tobacco plants enhanced cadmium accumulation. Int. J. Biol. Macromol. 116, 676–682. https://doi.org/10.1016/j.ijbiomac.2018.05.053.
Zhang, L., Gao, C., Mentink-Vigier, F., Tang, L., Zhang, D., Wang, S., Cao, S., Xu, Z., Liu, X., Wang, T., Zhou, Y., Zhang, B., 2019. Arabinosyl deacetylase modulates the arabinoxylan acetylation profile and secondary wall formation. Plant Cell 31, 1113–1126. https://doi.org/10.1105/tpc.18.00894.
Zhang, T-Y, Qian, Y-Q, Liu, Y-J, Wang, X., Yuan, Y-H, Yu, J., Wei, Y-Y, Wang, J., Li, B-Y, Qiao, Y-F, Du, L., Xu, M., Fu, A-G, 2025. The Cpn20-mediated plastid integrity is essential for growth and female gametophyte development in *Arabidopsis*. New Phytol. 247, 2746–2765. https://doi.org/10.1111/nph.70385.
Zhang, Y., Zhang, A., Li, X., Lu, C., 2020. The role of chloroplast gene expression in plant responses to environmental stress. Int. J. Mol. Sci. 21, 6082. https://doi.org/10.3390/ijms21176082.
Zulfiqar, U., Jiang, W., Xiukang, W., Hussain, S., Ahmad, M., Maqsood, M.F., Ali, N., Ishfaq, M., Kaleem, M., Haider, F.U., Farooq, N., Naveed, M., Kucerik, J., Brtnicky, M., Mustafa, A., 2022. Cadmium phytotoxicity, tolerance, and advanced remediation approaches in agricultural soils; a comprehensive review. Front. Plant Sci. 13. https://doi.org/10.3389/fpls.2022.773815.
Zúñiga-Sánchez, E., Soriano, D., Martínez-Barajas, E., Orozco-Segovia, A., Gamboa-deBuen, A., 2014. BIIDXI, the At4g32460 DUF642 gene, is involved in pectin methyl esterase regulation during *Arabidopsis thaliana* seed germination and plant development. BMC Plant Biol. 14, 338. https://doi.org/10.1186/s12870-014-0338-8.